



PGE1 and PGA1 bind to Nurr1 and activate its transcriptional function

Sreekanth Rajan^{1,15}, Yongwoo Jang^{1,2,3,15}, Chun-Hyung Kim^{2,4,15}, Woori Kim^{2,15}, Hui Ting Toh^{1,5}, Jeha Jeon², Bin Song², Aida Serra¹, Julien Lescar^{1,6}, Jun Yeob Yoo¹, Serap Beldar¹, Hong Ye¹, Congbao Kang⁷, Xue-Wei Liu⁸, Melissa Feitosa², Yeahan Kim², Dabin Hwang², Geraldine Goh⁹, Kah-Leong Lim^{9,10}, Hye Min Park¹¹, Choong Hwan Lee¹¹, Sungwhan F. Oh¹², Gregory A. Petsko¹³, Ho Sup Yoon^{1,6} ✉ and Kwang-Soo Kim^{1,2,14} ✉

The orphan nuclear receptor Nurr1 is critical for the development, maintenance and protection of midbrain dopaminergic (mDA) neurons. Here we show that prostaglandin E1 (PGE1) and its dehydrated metabolite, PGA1, directly interact with the ligand-binding domain (LBD) of Nurr1 and stimulate its transcriptional function. We also report the crystallographic structure of Nurr1-LBD bound to PGA1 at 2.05 Å resolution. PGA1 couples covalently to Nurr1-LBD by forming a Michael adduct with Cys566, and induces notable conformational changes, including a 21° shift of the activation function-2 helix (H12) away from the protein core. Furthermore, PGE1/PGA1 exhibit neuroprotective effects in a Nurr1-dependent manner, prominently enhance expression of Nurr1 target genes in mDA neurons and improve motor deficits in 1-methyl-4-phenyl-1,2,3,6-tetrahydropyridine-lesioned mouse models of Parkinson's disease. Based on these results, we propose that PGE1/PGA1 represent native ligands of Nurr1 and can exert neuroprotective effects on mDA neurons, via activation of Nurr1's transcriptional function.

Nuclear receptors (NRs) are, in general, classified as a superfamily of ligand-regulated transcription factors^{1,2}. However, for approximately half of the NR superfamily members, the physiological ligands are unknown and hence they are referred to as orphan nuclear receptors (ONRs)^{2,3}. Nurr1 is an ONR belonging to the NR4A subfamily, comprising NR4A1, NR4A2 and NR4A3 (also known as Nur77, Nurr1 and Nor1)^{4,5}. Nurr1 is critical for the development⁶ and maintenance of mDA neurons⁷, at least in part by inducing genes that are essential for dopamine (DA) synthesis and uptake as well as survival (for example, those for tyrosine hydroxylase (TH), aromatic amino acid decarboxylase (AADC), dopamine transporter (DAT) and glial cell line-derived neurotrophic factor receptor, c-Ret kinase). Moreover, Nurr1 protects mDA neurons from inflammation-induced cell death⁸. Furthermore, Nurr1's expression is notably diminished in the substantia nigra (SN) of postmortem brains of patients who had Parkinson's disease (PD)^{9,10}, suggesting that Nurr1 is a potential therapeutic target for PD^{11–13}. Thus, further insight into the signaling pathways regulating Nurr1's function is of great importance for future studies and treatments of PD.

Despite the critical biological functions of the NR4A family members, no endogenous/native ligands have been identified and

they have been designated as ONRs. They have also been considered constitutively active and ligand-independent^{4,5}, which was supported by a crystal structure showing that Nurr1-LBD adopts a conformation similar to that of agonist-bound, transcriptionally active NR-LBDs and lacks a 'classical' binding pocket due to the presence of bulky hydrophobic sidechain residues¹⁴. However, several studies suggested the possibility that NR4A members have native or synthetic ligands that regulate their transcriptional functions. For instance, PGA2 was found to interact with Nor1-LBD or Nur77-LBD and activate their transcriptional function^{15,16}. In addition, unsaturated fatty acids such as docosahexaenoic acid appear to bind to the LBDs of Nur77 (ref. 17) and Nurr1 (ref. 18). A recent study suggested that Nurr1's putative ligand-binding pocket is dynamic with high solvent accessibility and can expand, allowing binding of native ligands¹⁹. In addition, two groups reported the identification of synthetic/natural product ligands that can activate Nur77 via its LBD^{20,21}. Furthermore, using Nurr1-LBD-based cotransfection assays, we identified small molecules (amodiaquine, chloroquine and glafenin) that activate Nurr1's transcriptional function via direct interaction with its LBD²², prompting us to hypothesize that there could be an as-yet-unidentified native ligand(s) for Nurr1, which can activate Nurr1 through its LBD.

¹School of Biological Sciences, Nanyang Technological University, Singapore, Singapore. ²Molecular Neurobiology Laboratory, Department of Psychiatry, McLean Hospital, Harvard Medical School, Belmont, MA, USA. ³Department of Biomedical Engineering, Hanyang University, Seoul, Korea. ⁴Paeon Biotechnology, Daejeon, Korea. ⁵Nanyang Institute of Technology in Health and Medicine, Interdisciplinary Graduate School, Nanyang Technological University, Singapore, Singapore. ⁶NTU Institute of Structural Biology, Nanyang Technological University, Singapore, Singapore. ⁷Experimental Drug Development Centre, Agency for Science, Technology and Research, Nanos, Singapore, Singapore. ⁸Division of Chemistry and Biological Chemistry, School of Physical and Mathematical Sciences, Nanyang Technological University, Singapore, Singapore. ⁹National Neuroscience Institute, Singapore, Singapore. ¹⁰Lee Kong Chian School of Medicine, Singapore, Singapore. ¹¹Department of Bioscience and Biotechnology, Konkuk University, Gwangjin-gu, Seoul, Republic of Korea. ¹²Department of Anesthesiology, Perioperative and Pain Medicine, Brigham and Women's Hospital, Harvard Medical School, Boston, MA, USA. ¹³Ann Romney Center for Neurologic Diseases, Department of Neurology, Brigham and Women's Hospital, Harvard Medical School, Boston, MA, USA. ¹⁴Program in Neuroscience and Harvard Stem Cell Institute, McLean Hospital, Harvard Medical School, Belmont, MA, USA. ¹⁵These authors contributed equally: Sreekanth Rajan, Yongwoo Jang, Chun-Hyung Kim, Woori Kim. ✉e-mail: hsyoon@ntu.edu.sg; kskim@mclean.harvard.edu

Results

Identification of PGE1 as a potential ligand of Nurr1. To test our hypothesis, we first checked whether homogenized mouse tissue extracts prepared from brain, lung, heart and kidney can enhance Nurr1's transcriptional activation function. Toward this goal, we employed cotransfection assays in a human neuroblastoma cell line (SK-N-BE(2)C) using reporter constructs as previously described²². We found that these tissue extracts robustly enhanced the transcription activation function of Nurr1-LBD (Fig. 1a). We then performed a series of purification steps to isolate the active component(s) (Extended Data Fig. 1a). Notably, Nurr1-enhancing activity was largely unaffected by boiling and acetone precipitation. It was mostly retained after ultrafiltration (with a molecular weight cut-off of 3,000), indicating the presence of a small molecule ligand(s). Subsequently, using high-performance liquid chromatography (HPLC) fractionation, we identified an enriched fraction (fraction 5), which we selected for mass spectrometry (MS) analysis, revealing multiple candidate molecules (Extended Data Fig. 1b,c). Among these, we found that PGE1 and 8-iso PGE1 prominently stimulate Nurr1-LBD reporter activity (Fig. 1b,c). Moreover, PGE1 enhanced the transcriptional activity of the full-length Nurr1 in a dose-dependent manner (Fig. 1d). Furthermore, coexpression of transcriptional coactivators (steroid receptor coactivator 1 (SRC1) and SRC3) potentiated PGE1-induced Nurr1 activation (Fig. 1e). We also investigated whether PGE1 can promote the recruitment of Nurr1, SRC1 and/or SRC3 to the Nurr1-binding motif located in the upstream TH gene promoter by chromatin immunoprecipitation (ChIP) assays. We found that treatment with PGE1 enhanced the recruitment of Nurr1, SRC1 and SRC3 to the NL3 site on the TH promoter (Fig. 1f). In line with this, treatment with PGE1 prominently augmented Nurr1's interaction with SRC1 or SRC3 in a coimmunoprecipitation (co-IP) assay (Fig. 1g).

Structural and biophysical characterization of the interactions between PGE1/PGA1 and Nurr1-LBD.

We next examined the molecular interaction between PGE1 and Nurr1-LBD by employing two-dimensional ¹H-¹⁵N heteronuclear single quantum correlation (HSQC) nuclear magnetic resonance (NMR) spectroscopy, before and after the addition of PGE1. Chemical shift perturbations (CSPs) were observed in residues located around helices H11 and H12 of Nurr1-LBD, such as Ser553, Lys554, Gly557, Thr564 and Gln571 (helix H11), Lys590, Phe592, Leu593, Asp594 and Thr595 (helix H12) (Extended Data Figs. 2a,b and 3a), showing that there is a direct physical interaction between PGE1 and Nurr1-LBD, mainly confined to helix H12. Next, we attempted to cocrystallize Nurr1-LBD with PGE1 and determine the structure of the complex. Cocrystals diffracted to 2.4 Å resolution. The structure revealed the dehydrated PGE1 metabolite, PGA1 (Fig. 1h), in the bound form (Extended Data Fig. 4a and Supplementary Table 1), forming a covalent adduct between the C11 atom of the cyclopentenone ring and the thiol group of Cys566 of the LBD. Thus, we tested the molecular interaction between PGA1 and Nurr1-LBD by NMR spectroscopy, showing that the PGA1-mediated perturbations are similar to those in the presence of PGE1 (Extended Data Figs. 2c,d and 3b). This suggests that PGE1 and PGA1 recognize the same binding region, localized around helices H11 and H12, in Nurr1-LBD. Furthermore, multiple residues such as Gly569, Lys590, Phe592 and Asp594, which shifted on PGA1/PGE1 binding, also revealed resonance line broadening phenomenon suggesting intermediate exchange on the NMR timescale, while additional peaks for residues such as Gln571, Leu559 and Thr595 were identified for the PGA1-bound form (Extended Data Figs. 2a,c and 3c,d). Furthermore, PGA1 also increased the transcriptional activities of both Nurr1-LBD and full-length Nurr1 (Extended Data Fig. 2e,f) in a dose-dependent manner in SK-N-BE(2)C cells. Also, treatment with PGA1 prominently augmented Nurr1's interaction with SRC1 or SRC3 (Fig. 1g).

Spontaneous dehydration of PGE1 to PGA1, yielding crystals of the Nurr1-PGA1 adduct, could have resulted from the crystallization conditions used (Extended Data Fig. 4b), as it is well known that PGE1 can be readily dehydrated to PGA1 in acidic/basic pH environment²³. To confirm this, Nurr1-LBD was cocrystallized with PGA1 as the starting compound, yielding improved crystals that allowed data to be collected to 2.05 Å resolution (Supplementary Table 2, Supplementary Video 1, Fig. 2a and Extended Data Fig. 5a,b), revealing an essentially identical covalent complex. Electron density corresponding to PGA1 was observed in Nurr1-LBD in a space surrounded by helices H4, H11 and H12, with the two hydrophobic tails of PGA1 splayed on binding to the protein (Fig. 2a, Extended Data Fig. 5b and Supplementary Table 3). One hydrophobic tail inserts deeply into a narrow hydrophobic cavity lined by residues Phe443, Leu444 (helix H4), Leu570, Ile573 (helix H11), Ile588, Leu591 and Phe592 (helix H12), while the carboxylic acid-bearing tail appears flexible and occupies different orientations in the two complexes present in the crystallographic asymmetric unit (Supplementary Fig. 1). PGA1 is stabilized by several hydrogen bonds and van der Waals interactions (Extended Data Fig. 5b and Supplementary Table 3). Residues Glu440, Leu444, Thr567 and Arg563 form hydrogen bonds with the hydroxyl oxygen and cyclopentenone ketone of PGA1, while residues His516 and Arg515 stabilize the carboxylic acid-bearing tail of PGA1 (Supplementary Table 3).

The most intriguing feature of Nurr1-LBD bound to PGA1 is the formation of a covalent bond (Fig. 2a and Extended Data Fig. 5b) between the cyclopentenone carbon C11 of PGA1 with the sulfur atom of Cys566, as a result of a Michael addition reaction, flipping the side chain of Cys566 by an angle of ~115° in comparison to its apo form. The covalent coupling of PGA1 with Nurr1-LBD was also confirmed by MS following the incubation of Nurr1-LBD with PGA1, while PGE1 did not form such a covalent complex (Fig. 2b). The mass for Nurr1-LBD, in the presence and absence of PGE1, was 30,525 Da, while the Nurr1-LBD-PGA1 complex mass shifted by an additional 336.5 Da, corresponding to that of PGA1 (Fig. 2b). A similar covalent adduct was previously observed in PPARγ-LBD in complex with a few fatty acids, including its endogenous ligand 15d-PGJ2 (ref. ²⁴). Attempts were made to examine the selectivity of prostaglandins, demonstrating that PGJ2 and 15d-PGJ2 had no effect on the transcriptional activities of Nurr1-LBD (Extended Data Fig. 5c). On the other hand, PGE1/PGA1 did not affect the transcriptional activities of PPARγ-LBD (Extended Data Fig. 5d) or those of PPARα-LBD, RXRα-LBD, LXR-LBD and GR-LBD (Supplementary Fig. 2a-d) suggesting that PGE1/PGA1 specifically activate the transcriptional function of Nurr1. In general, the prostaglandin A and J series contain a cyclopentenone ring, which possesses an α,β-unsaturated carbonyl group with an electrophilic center susceptible to form a covalent bond (Michael adduct) with a nucleophile such as the thiolate anion formed by deprotonation of the thiol group of Cys residues. In addition, most PGJ analogs possess a second electrophilic center in their hydrophobic tails (Supplementary Fig. 2e,f). In the Nurr1-LBD-PGA1 structure, the cyclopentenone carbon C11 in PGA1 covalently attaches to Cys566 in Nurr1-LBD, forming a narrow groove where one of the hydrophobic tails of PGA1 orients itself, while the carboxyl group bearing tail is exposed to the surface (Extended Data Fig. 5b). On the other hand, the hydrophobic tail carbon C13 in 15d-PGJ2 is covalently attached to Cys285 in PPARγ-LBD, but is completely embedded within its classical binding cavity (Supplementary Fig. 2e,f). These subtle differences in chemical and conformational constraints, together with the transcriptional activity analysis (Extended Data Fig. 5c,d and Supplementary Fig. 2), explain the observed specificity of PGA1 toward Nurr1.

Functional characterization of interacting residues of the Nurr1-LBD. The importance of the interacting residues was validated by site-directed mutagenesis. Mutation of Thr567, forming a

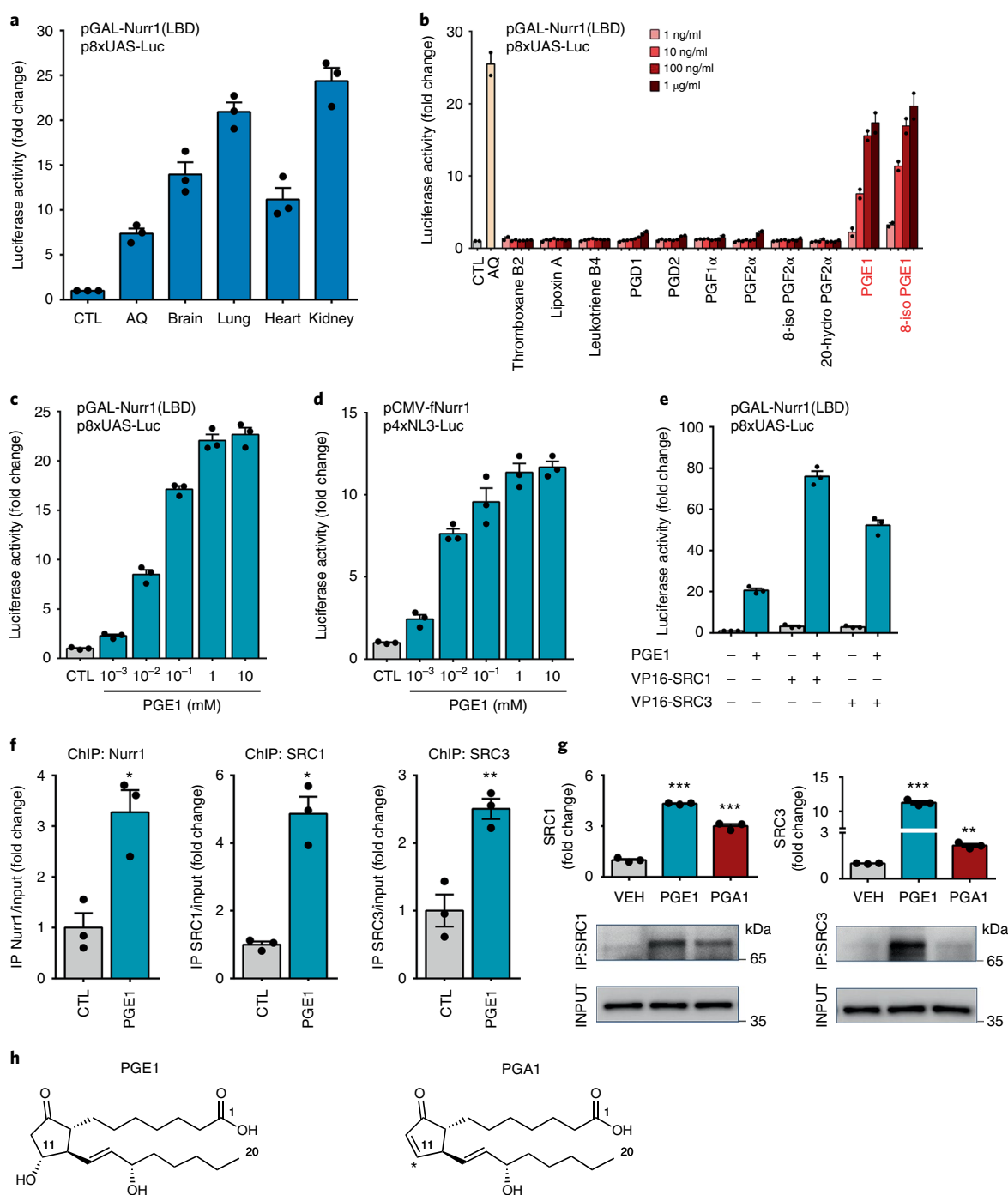


Fig. 1 | Identification of PGE1 and 8-iso-PGE1 as Nurr1 activators from brain tissue extracts. **a**, Brain, lung, heart and kidney tissue extracts increase the transcriptional activity of Nurr1-LBD-based reporter constructs. Amodiaquine (AQ) (10 μ M) was used as positive control. $n=3$ independent experiments. Data are presented as mean \pm s.d. **b**, PGE1 and 8-iso PGE1 increase transcriptional activity of Nurr1-LBD in a dose-dependent manner. Amodiaquine (30 μ M) was used as positive control. $n=2$ independent experiments. Data are presented as mean \pm s.d. **c,d**, PGE1 also induces Nurr1-LBD-dependent (**c**) and full-length Nurr1-dependent (**d**) transcriptional activity in a dose-dependent manner. $n=3$ independent experiments. Data are presented as mean \pm s.e.m. **e**, PGE1 (1 μ M)-induced Nurr1 activation is potentiated by transcriptional coactivators, SRC1 and SRC3 in SK-N-BE(2)C cells. $n=3$ independent experiments. Data are presented as mean \pm s.e.m. **f**, ChIP assay using antibodies against Nurr1, SRC1 and SRC3 in rat pheochromocytoma PC12 cells untreated or treated with PGE1 (1 μ M). The TH promoter sequence including the Nurr1 binding site (NL3) was detected by rtPCR. The treatment of PGE1 significantly increases the binding on NL3 sequence of Nurr1 (3.27 ± 0.44 , $P=0.017$), SRC1 (4.86 ± 0.50 , $P=0.015$) and SRC3 (2.50 ± 0.15 , $P=0.009$). $n=3$ independent experiments. Data are presented as mean \pm s.e.m., * $P < 0.05$, ** $P < 0.01$, two-tailed Welch's t -test. **g**, Co-IP assays show that treatment with PGE1 (1 μ M) augments Nurr1's interaction with SRC1 (4.33 ± 0.03) or SRC3 (11.24 ± 0.24) in SK-N-BE(2)C cells. The application of PGA1 (10 μ M) also increases Nurr1's interaction with SRC1 (3.00 ± 0.12) or SRC3 (2.16 ± 0.12). $n=3$ independent experiments. Data are presented as mean \pm s.e.m., ** $P < 0.01$, *** $P < 0.001$ (one-way ANOVA, Tukey's post hoc test). **h**, Chemical diagram of PGE1 and PGA1 indicating the Michael addition center (*, C11) in PGA1, which is attached to a hydroxyl group in PGE1.

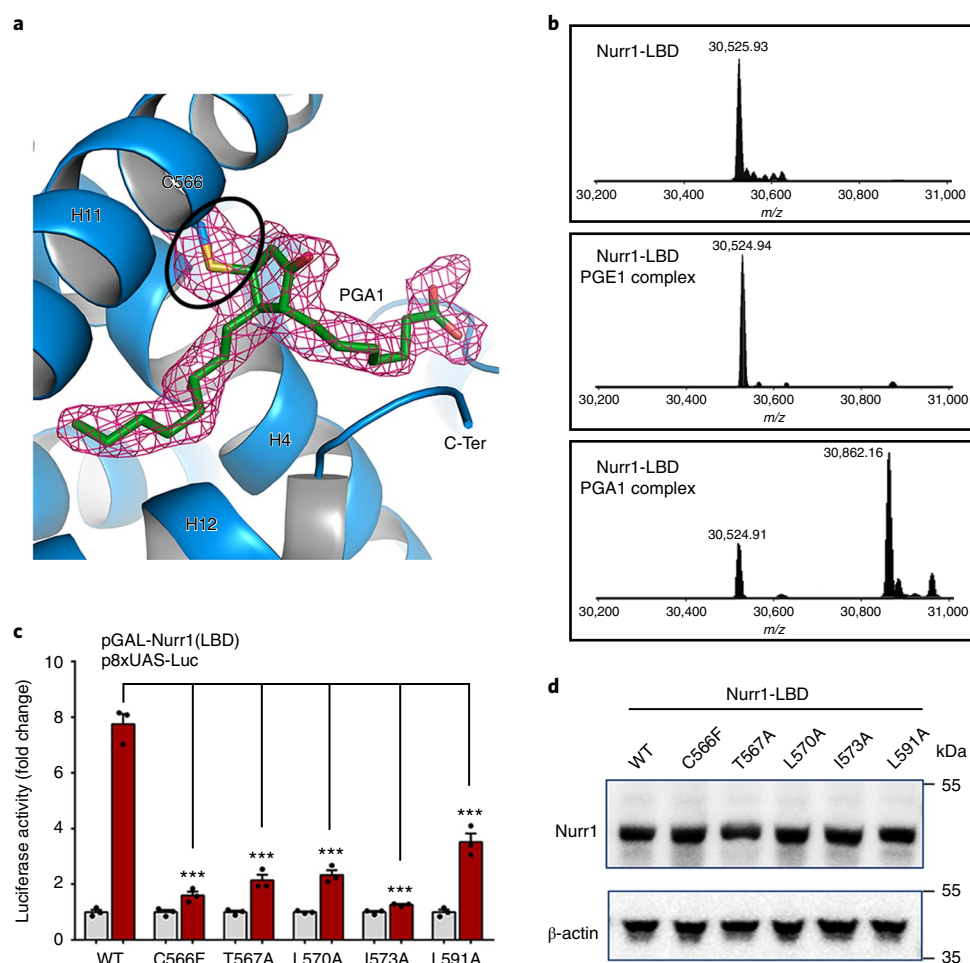


Fig. 2 | Crystal structure of PGA1-bound Nurr1-LBD and its molecular and functional analyses. **a**, The 2Fo-Fc electron density map (pink color) contoured at 1σ cut-off clearly reveals the covalent bond (within black circle) between the sulfur of Cys566 and cyclopentenone C11 of PGA1, as well as the well-ordered PGA1 packed between helices H4, H11 and H12. **b**, MS data confirming that PGA1 is covalently attached to Nurr1-LBD. The MS data for apo (top), PGE1 (middle) and PGA1 (bottom) bound Nurr1-LBD, reveals the presence of covalent complex formation in the presence of PGA1 but not PGE1, as shown by the combined molecular mass of 30,862 Da (Nurr1-LBD³²⁸⁻⁵⁹⁸ is 30,525 Da and PGA1 is 336.5 Da). **c**, Functional effects of mutations in the potential PGA1 binding residues on Nurr1's transcriptional activity. Wild-type (WT) and mutant constructs (C566F, T567A, L570A, I573A or L591A) were examined by luciferase reporter assay with or without PGA1 (10 μ M). The mutant constructs show a significant reduction in Nurr1's transcriptional activity. The mean and error values are as following: WT (7.75 \pm 0.37), C566F (1.59 \pm 0.14), T567A (2.14 \pm 0.20), L570A (2.32 \pm 0.18), I573A (1.26 \pm 0.03) and L591A (3.52 \pm 0.31). $n = 3$ independent experiments, Data are presented as mean \pm s.e.m., *** $P < 0.001$ compared with PGA1-treated WT (one-way ANOVA, Tukey's post hoc test). **d**, Mutations do not affect the protein expression levels. $n = 3$ independent experiments.

hydrogen bond with the ketone attached to the cyclopentenone ring of PGA1, robustly diminished PGA1-induced transcriptional activities of Nurr1-LBD, while mutation of Arg563, His516 and Arg515 did not (Fig. 2c,d and Extended Data Fig. 6a), probably owing to the flexibility in their sidechain conformations combined with that of the carboxyl tail of PGA1. However, mutations of residues (Leu570, Ile573 and Leu591, except for Phe443) conferring nonpolar interactions mostly diminished PGA1-induced transcriptional activities of Nurr1-LBD (Fig. 2c and Extended Data Fig. 6b). In the case of Cys566, its mutation to Phe or His in comparison to Ala (Extended Data Fig. 6c) influenced Nurr1's PGA1-induced transcriptional activities, suggesting that it exerts a stereo-specific requirement for certain amino acids to interact with PGA1. Thus, the interacting amino acids (for example, Cys566, Thr567, Leu570, Ile573 and Leu591) are critical for PGA1-induced transcriptional activities of Nurr1-LBD without affecting their protein levels (Fig. 2c,d).

A structural comparison of the Nurr1-LBD-PGA1 complex with the apo protein revealed that on complex formation, the H12 helix, encompassing the activation function-2 (AF-2) region,

is reoriented away from the core of the protein by an angle of 21° (Fig. 3a and Supplementary Video 2), due to the direct interactions with the ligand. Minor conformational changes are also observed in the H11-H12 (Asp580-Pro583) and H8-H9 (Val512-Glu520) loop regions. The movement of H12 alters several charged interactions in this region (Supplementary Table 4): the salt-bridge between Glu440 in H4 and Lys590 in H12 (a distance of 2.8 Å in the apo structure) becomes disrupted (new distance, 6.0 Å) in the PGA1-bound form (Fig. 3b and Supplementary Table 4). Another salt-bridge between Lys590 and Asp594 is also lost on PGA1 binding. Conformational changes are also observed near the carboxylate end of PGA1, where the sidechain of Arg563 flips by ~60° in comparison to the apo structure. This relieves the interactions made by Arg563 with its neighboring residues (Supplementary Table 4), perhaps providing some driving force for the conformational changes to enable PGA1 binding. Moreover, the sidechain of Glu514 flips by ~94°; as a result, it is displaced by ~8 Å from Arg563 (Fig. 3c and Supplementary Table 4). It is to be noted that these two residues adopt flexible orientations within the two chains in the

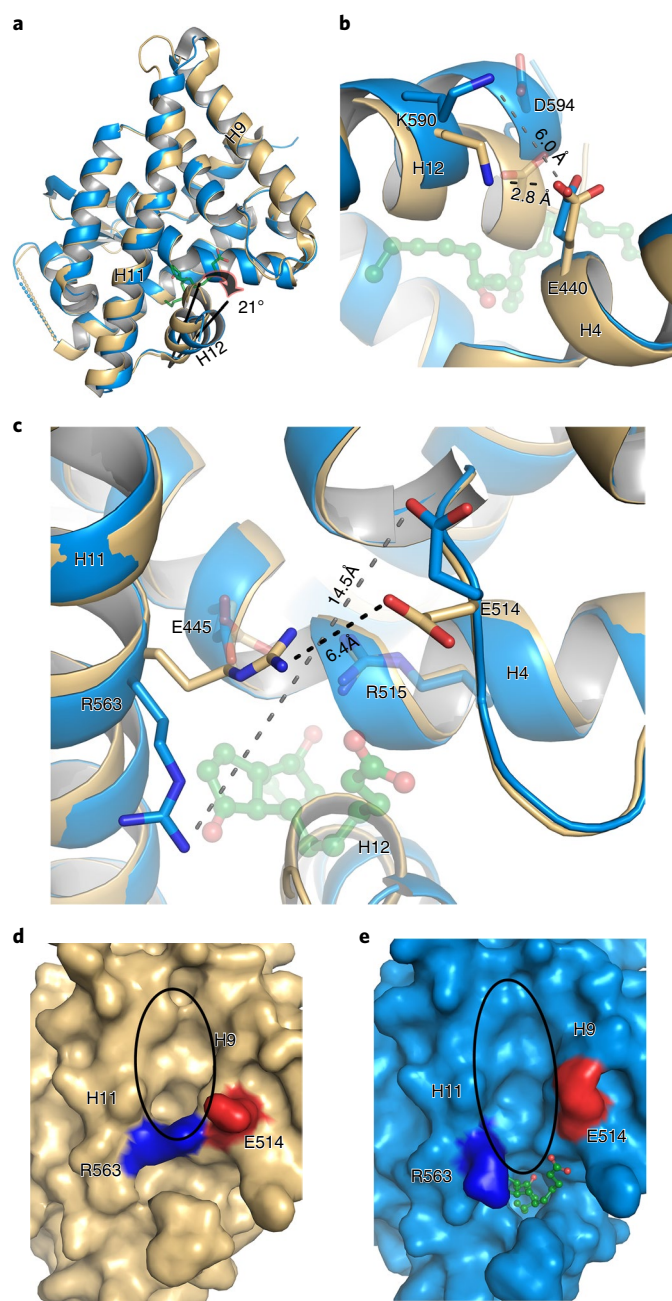


Fig. 3 | Structural comparison of apo and PGA1-bound Nurr1-LBD.

a, Cartoon representation of the superposition of the PGA1 bound to Nurr1 (blue) with its apo form (pale yellow) revealing a shift of the helix H12 by 21° away from the protein core, enabling the binding of PGA1 shown in stick mode. **b**, PGA1 binding leads to a ~3.0 Å expansion of the salt-bridge between residues Glu440 and Lys590. **c–e**, Similarly, the distance between residues Glu514 and Arg563 also expands by ~8 Å (**c**). As a result, the surface pocket area formed by the H9–H11 wedge enlarges considerably in the PGA1 bound form (**e**) in comparison with the apo form (**d**).

asymmetric unit, as well as in the apo structure. In any case, the overall conformation of these two residues, Glu514 and Arg563, in the apo form indicates that they act as gatekeepers blocking the surface pocket formed by the wedge between helices H9 and H11 (Fig. 3d). In contrast, in the Nurr1–PGA1 complex, we find an expansion of this H9–H11 wedge region (Fig. 3e), indicating that this region is a probable interface for coregulator binding²⁵ or RXR heterodimerization²⁶ (Supplementary Fig. 3), corroborating

that PGA1 binding affects the network of interactions involving charged residues (Glu440, Glu445, Glu514, Arg515, Arg563, Lys590 and Asp594) around this region (Supplementary Table 4 and Supplementary Video 2). Although PGA1 binding induces a notable movement in helix H12 of Nurr1, the classical active site residues are virtually unperturbed (Supplementary Fig. 4). Of the 14 residues at this site, only three (Leu444, Ile573 and Leu591) interact with PGA1, of which only Leu591 undergo conformational changes, mainly owing to the H12 movement. This indicates that Nurr1 activation is mostly governed by the reorientation of H12. Besides, from an analysis of the Nur77–ligand complexes^{27–30}, it was apparent that the ligands occupied the surface near the helix H12 and along the H9–H11 wedge (Supplementary Fig. 5a,b). In analogy with the Nurr1–PGA1 complex, it could be perceived that this ligand-binding region could be unique to the NR4A family, unlike other nuclear receptors. The superposition of Nur77–LBD with Nurr1–LBD also revealed that the helix H12 reorientation leads to a similar orientation among the ligand-bound LBDs (Supplementary Fig. 5c), in comparison to the apo Nurr1–LBD where it is in a closed conformation.

Comparative studies of PGE1 and PGA1 for their binding properties and transcriptional activation functions. It is well known that PGEs play their diverse biological functions through G-protein-coupled PGE receptors (that is, EP1–4)³¹. In particular, EP2 is prominently expressed in neuronal cells and appears to play important roles for their neuroprotection^{32,33}. In agreement with these studies, we found that an EP2 agonist (AH13205), but not EP3/EP4 agonists (Sulprostone and CAY10598) activated Nurr1's transcriptional function (Extended Data Fig. 7a). Besides, among specific antagonists of EP1 (SC-19220), EP2 (PF-04418948), EP3 (L-798106) and EP4 (L-161982), only the EP2 antagonist prominently attenuated PGE1-induced Nurr1 transcriptional activation (Extended Data Fig. 7b). Also, the PGE1 synthetic agonist misoprostol activated Nurr1 in a dose-dependent manner (Extended Data Fig. 7c). To compare PGA1/PGE1's binding affinities to EP2 and Nurr1–LBD, we next conducted radiolabeled ligand-binding and competition assays using [³H]-PGE1 and [³H]-PGA1 (Fig. 4). Both [³H]-PGE1 and [³H]-PGA1 showed saturable binding to Nurr1–LBD (Fig. 4a,c). It is noted that the saturation assays and NMR titration data (Supplementary Fig. 6) showed a difference in binding constants, which may be attributable to different experimental conditions^{34,35}. Moreover, competition assays showed that unlabeled PGE1 and PGA1 could compete with [³H]-PGE1 and [³H]-PGA1 for binding to Nurr1–LBD (Fig. 4b,d). In contrast, unlabeled 15d-PGJ2 and retinoic acid (ligands for PPARγ and retinoid acid receptor, respectively) failed to compete with neither [³H]-PGE1 nor [³H]-PGA1 for binding to Nurr1–LBD (Fig. 4b,d), showing that PGA1/PGE1's binding to Nurr1–LBD is highly specific. Misoprostol competed with [³H]-PGE1 (Fig. 4b). Next, we performed EP2 receptor binding assays using [³H]-PGE1 and [³H]-PGA1. While [³H]-PGE1 exhibited saturable binding to EP2, [³H]-PGA1 did not bind to EP2 (Fig. 4e,f). Consistent with these results, cold PGA1, as well as 15d-PGJ2, failed to compete with [³H]-PGE1 for its binding to EP2 while cold PGE1 and misoprostol were able to (Fig. 4g). In sum, these data demonstrate that both PGE1 and PGA1 directly and comparably bind to Nurr1–LBD, while only PGE1, but not PGA1, interacts with EP2.

Notably, PGE1 activated Nurr1's transcriptional function with much higher efficiency than PGA1 in SK-N-BE(2)C cells (Fig. 1c,d and Extended Data Fig. 2e,f). Since these cells are not of mDA origin, we next tested PGE1 and PGA1 in two mDA cell lines, MN9D and N27-A, originating from mouse and rat mesencephalic mDA neurons, respectively^{36,37}. PGE1 and PGA1 increased transcriptional function of both Nurr1–LBD and full-length Nurr1, and PGE1's potency was approximately twofold higher than PGA1 in both cell

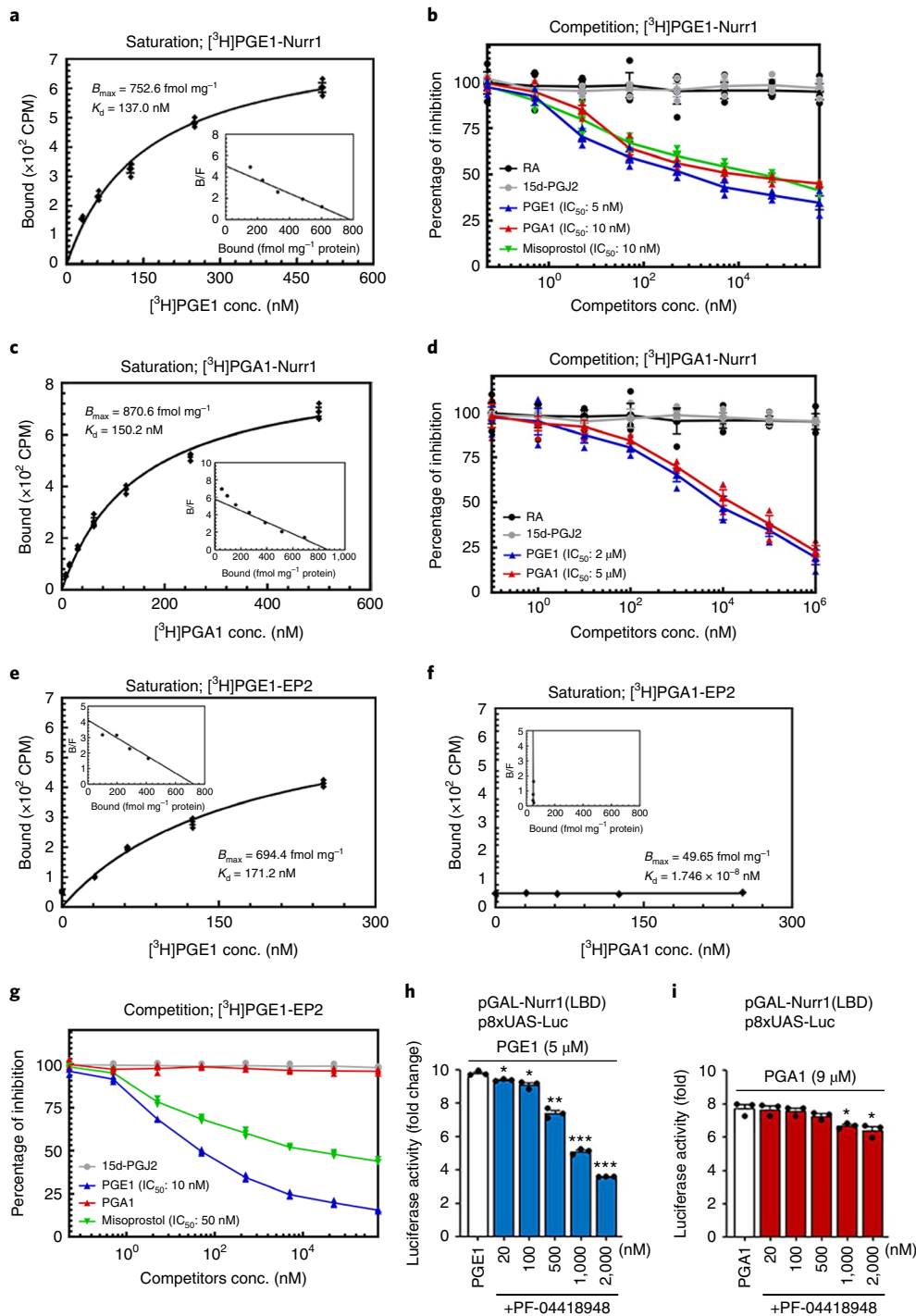


Fig. 4 | Direct binding of PGE1/PGA1 to Nurr1-LBD or EP2. **a-d**, Saturation and competition assays of PGE1/PGA1 with Nurr1-LBD. **a**, Nurr1-LBD protein was incubated with increasing concentrations (31.3, 62.5, 125, 250 and 500 nM) of [³H]-PGE1 for saturation assay. The inset indicates Scatchard analysis of the specific binding. **b**, Competition of PGE1, PGA1, misoprostol, 15d-PGJ2 or retinoic acid for binding of [³H]-PGE1 to Nurr1-LBD. Increasing concentrations of unlabeled competitors were incubated with 500 nM of [³H]-PGE1 and 0.2 μ M of Nurr1-LBD. **c**, Similar to [³H]-PGE1, Nurr1-LBD was incubated with 7.8, 15.6, 31.3, 62.5, 125, 250 and 500 nM of [³H]-PGA1. **d**, Unlabeled PGE1, PGA1, 15d-PGJ2 or retinoic acid were incubated with 1 μ M of [³H]-PGA1 and 0.2 μ M of Nurr1-LBD for competition assay. $n = 3$ independent samples per group. Data are mean \pm s.e.m. **e-g**, Saturation and competition assays of PGE1/PGA1 with EP2. **e,f**, EP2 protein (0.38 μ M) was incubated with 31.25, 62.5, 125 and 250 nM of [³H]-PGE1 (**e**) or [³H]-PGA1 (**f**) for saturation assay. Contrary to [³H]-PGE1, [³H]-PGA1 does not interact with EP2. **g**, Competition of PGE1, PGA1, misoprostol or 15d-PGJ2 for binding of [³H]-PGE1 to EP2. $n = 3$ independent samples per group. Data are mean \pm s.e.m. **h,i**, PF-04418948 effectively inhibits PGE1-induced transcriptional activity of Nurr1 in MN9D cells (**h**). PF-04418948 only marginally inhibits PGA1-induced transcriptional activity of Nurr1 in MN9D cells (**i**). * $P < 0.05$, ** $P < 0.01$, *** $P < 0.001$ compared to PGE1/PGA1 only, unpaired two-tailed t -test; $n = 3$ independent samples per group. Data are mean \pm s.e.m.

lines, as examined by the half-maximal effective concentration (EC_{50}) (Supplementary Fig. 7a,b). To further test whether PGE1, but not PGA1, can activate the transcriptional activity of Nurr1 via EP2, we next tested the effects of treatment with PF-04418948, which is a highly selective EP2 antagonist³⁸. Indeed, PF-04418948 suppressed PGE1-induced transcriptional activation of Nurr1 in a dose-dependent manner both in MN9D (Fig. 4h) and N27-A cell lines (Supplementary Fig. 7c). In contrast, PF-04418948 had a marginal effect on PGA1-induced activation both in MN9D (Fig. 4i) and N27-A cell lines (Supplementary Fig. 7d).

Biological importance of PGE1/PGA1 using in vitro and in vivo models. We then investigated the potential biological function(s) of the PGE1/PGA1-Nurr1 axis using in vitro and in vivo models of PD. First, we examined PGE1/PGA1's neuroprotective effects on neurotoxin-induced cell lines. Treating SK-N-BE(2)C cells with the dopaminergic selective neurotoxin, 1-methyl-4-phenylpyridinium (MPP⁺), generated from the precursor 1-methyl-4-phenyl-1,2,3,6-tetrahydropyridine (MPTP), resulted in robust increases in oxidative stress levels as examined by the reporter DCFH-DA (2',7'-dichlorofluorescein diacetate), which emits fluorescence on interaction with reactive oxygen species (Supplementary Fig. 8b). Notably, treatment with PGE1/PGA1 (1 and 5 μ M, respectively) significantly decreased levels of DCF fluorescence. Treatment with PGE1/PGA1 combined with Nurr1 overexpression potentiated PGE1/PGA1's effect and further reduced both DCF fluorescence and MPP⁺-induced cytotoxicity (Supplementary Figs. 8a-c and 9a). PGE1/PGA1's neuroprotective effects disappeared when Nurr1 was knocked down (Supplementary Figs. 8d,e and 9b). In addition, overexpression of wild-type Nurr1, but not that of mutant forms (for example, C566F and T567A) could significantly decrease MPP⁺-induced cytotoxicity (Supplementary Fig. 8f). We also tested the effect of PGE1/PGA1 treatment on MPP⁺-induced cytotoxicity and cell death in MN9D and N27-A cells, together with overexpression or knockdown of Nurr1. As shown in Extended Data Fig. 8 (MN9D) and Supplementary Fig. 10 (N27-A), MPP⁺ treatment induced significant cell death and cytotoxicity in both cell lines and treatment with PGE1 or PGA1 exhibited significant neuroprotective effects. These PGE1/PGA1 neuroprotective effects (at 3 and 5 μ M, respectively) were enhanced by Nurr1 overexpression but completely disappeared when Nurr1 was knocked down (Fig. 5a-d). Furthermore, we found that MPP⁺ treatment prominently decreased DA-related gene expression (for example, TH, DAT, AADC, vesicular monoamine transporter 2 (VMAT2), paired-like homeodomain 3 (Pitx3) and c-Ret), which was significantly rescued by PGE1/PGA1 treatment in MN9D cells (Supplementary Fig. 11). When Nurr1 was knocked down, basal expression of these genes was significantly reduced and PGE1/PGA1 were unable to rescue the reduced gene expression. Moreover, PGE1/PGA1 treatment resulted in a significant increase of DA levels in MN9D cells, both in the absence and in the presence of MPP⁺ treatment, in a Nurr1-dependent manner (Supplementary Fig. 12).

Next, to investigate the neuroprotective effects of PGE1/PGA1 in a more physiological context, we employed a primary mDA neuron-glia coculture system derived from the embryonic day 14 (E14) rat ventral mesencephalic area. Treatment with MPP⁺ (0.5 μ M) or lipopolysaccharide (LPS; 15 ng ml⁻¹) prominently decreased the number of TH⁺ mDA neurons by more than 60% (Fig. 5e,f). Moreover, the remaining mDA neurons exhibited abnormal morphology, including shortened and/or fragmented neurites. Also, LPS treatment resulted in robust microglial activation, as evidenced by Iba-1 immunostaining (Fig. 5e). Notably, treatment with PGE1 (Fig. 5f) or PGA1 (Fig. 5g) significantly rescued both MPP⁺- and LPS-induced loss of mDA neurons when >10 nM was used, suggesting that PGE1/PGA1 may work in physiological contexts. In line with this, both PGE1 and PGA1 were detected by enzyme-linked

immunosorbent assay (ELISA) in mouse brain areas, including the midbrain and the striatum at the ranges of 5–25 pg mg⁻¹, which correspond to approximately 15–70 nM (Supplementary Fig. 13a). PGE1 levels were higher than PGA1, and PGA1 levels were higher in the striatum and the midbrain areas than in the hippocampus and the cerebellum. Moreover, stereotactic injection of PGE1/PGA1 (2 μ g ml⁻¹) to the SN resulted in a significant upregulation of messenger RNA levels of Nurr1's target genes (for example, TH, DAT, AADC and VMAT2) (Supplementary Fig. 13b) as well as in upregulation of DA levels (Supplementary Fig. 13c,d), compared to the vehicle-injected side.

Finally, we tested the in vivo effect of PGE1/PGA1 in a subchronic MPTP-induced animal model of PD. Mice were treated with PGE1 or PGA1 (2 mg kg⁻¹), starting from 3 d before subchronic MPTP regimen (30 mg kg⁻¹ d⁻¹, 5 d) and continuing until day 8 (Fig. 6a). MPTP treatment resulted in significant bodyweight loss, starting from the third day of injection, compared to vehicle (VEH) treatment. Notably, cotreatment with PGE1 or PGA1 prevented MPTP-induced body weight loss throughout the whole regimen (Supplementary Fig. 14). Motor behavior was assessed using the rotarod, pole test and cylinder tests in an assessor- and observer-blinded fashion. MPTP-treated mice showed significantly impaired motor behavior in all three tests compared to VEH-treated mice, when tested following subchronic MPTP administration (Fig. 6b-d). Both PGE1 and PGA1 significantly recovered MPTP-induced motor deficits in the rotarod and pole tests by increasing the latency to fall on a rotating rod and by reducing the time to traverse on a pole (Fig. 6b,c). In addition, PGE1 significantly rescued the number of rearing events in the cylinder test compared to MPTP treatment (Fig. 6d). Albeit statistically insignificant, PGA1 also tended to increase the number of rearing events. Furthermore, additional blinded immunohistochemical analyses demonstrated that TH⁺ and NeuN⁺ neurons were significantly retained in the SN of PGE1 or PGA1-treated mice together with higher TH density in the striatum, compared to VEH-treated control mice (Fig. 6e-i). PGE1/PGA1 significantly restored DA levels both in the SN and in the striatum (Extended Data Fig. 9a,b). We also found a similar neuroprotective effect of PGE1 and PGA1 in an acute MPTP mouse model (Supplementary Fig. 15). Acutely MPTP-treated mice showed impaired motor behavior in latency to fall on a rotating rod and time to descent on the pole, compared to saline-treated mice, when tested on day 6 following MPTP administration. PGE1/PGA1 administration significantly ameliorated MPTP-induced behavioral deficits on both the rotarod and pole tests (Supplementary Fig. 15b,c), and this improvement was accompanied by a significant sparing of TH⁺ neurons in the SN and TH density in the striatum (Supplementary Fig. 15d-g), compared to saline-treated control mice.

Discussion

Prostaglandins were first isolated from semen in the 1930s, and their structures were elucidated in the 1960s³⁹, thereafter opening up an extensive research era in the field. In the present study, although Nurr1 has been widely considered to be a constitutively active, ligand-independent ONR^{4,5}, we provide multiple lines of evidence supporting the notion that PGE1/PGA1 are native/endogenous ligands of Nurr1. They can directly interact with Nurr1-LBD, prominently regulate its transcriptional activity, exhibit neuroprotective cellular effects in a Nurr1-dependent manner, considerably rescue both MPP⁺- and LPS-induced losses of TH⁺ mDA neurons and spare the number of mDA neurons in the SN as well as TH density in the striatum, leading to improvement of motor behavioral deficits. Based on these data, we propose that PGE1/PGA1 represent native ligands of Nurr1, exerting their neuroprotective effects in PD models via Nurr1 activation.

A salient feature of our study is that PGA1, but not PGE1, forms a covalent bond with Nurr1-LBD by a Michael addition reaction,

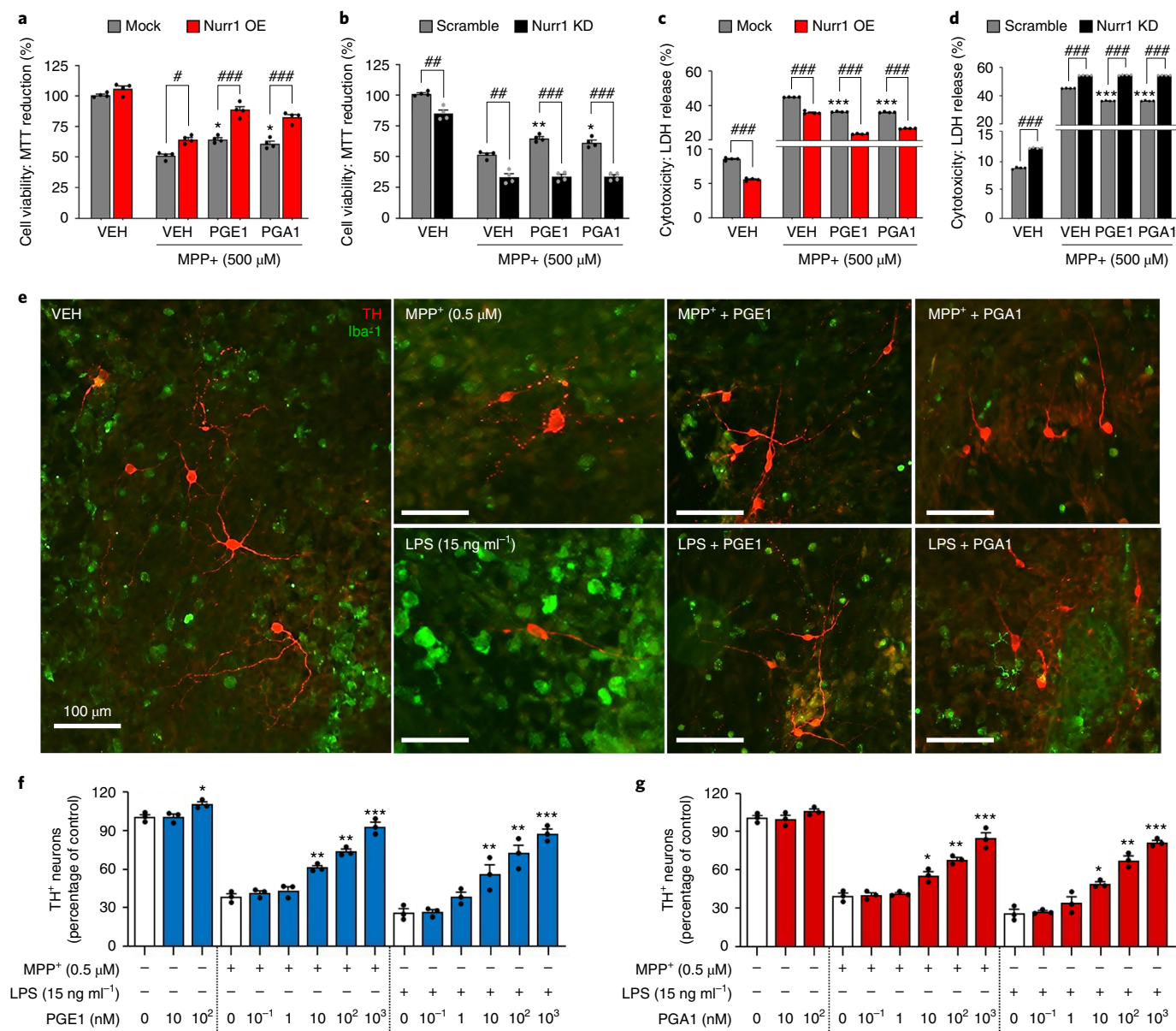


Fig. 5 | Neuroprotective effect of PGE1/PGA1 is dependent on Nurr1. **a–d**, Protective effects of PGE1 and PGA1 on cell viability and cytotoxicity measured by MTT reduction and LDH release in MN9D cells. Nurr1 overexpression (OE) potentiates the protective effects of PGE1 (3 μ M) and PGA1 (5 μ M) both in the normal condition and MPP⁺-induced toxic condition compared to Mock OE (**a,c**). Nurr1 knockdown (KD), however, attenuates PGE1/PGA1's protective effects under both normal and MPP⁺-induced toxic conditions (**b,d**). * $P < 0.05$, *** $P < 0.001$ compared to VEH treatment under Mock or Scramble conditions; # $P < 0.05$, ## $P < 0.01$, ### $P < 0.001$ compared between each treatment group, one-way ANOVA, Tukey's post hoc test; $n = 4$ independent samples per group. Data are mean \pm s.e.m. **e–g**, PGE1 (**e,f**) or PGA1 (**e,g**) treatment ameliorates both MPP⁺- and LPS-induced losses of TH-positive mDA neurons at nanomolar ranges in primary mDA-glia cocultures isolated from rat embryonic ventral mesencephalic area. Scale bars in **e**, 100 μ m. * $P < 0.05$, ** $P < 0.01$, *** $P < 0.001$ compared to 0 nM, unpaired two-tailed t -test; $n = 3$ biologically independent samples per group. Data are mean \pm s.e.m. from two biologically independent experiments.

a result validated by MS (Fig. 2b and Extended Data Fig. 10). The crystallization conditions could trap only the covalently bound PGA1 to Nurr1, resulting in a Cys566 sidechain flip, and this Cys566 flexibility might also accommodate the additional hydroxyl group in PGE1. Moreover, the crystal structure enabled us to explain the molecular basis of Nurr1 activation by PGA1, which is mainly governed by reorientation of the H12 helix and other subtle conformational changes, in a manner unlike classical NR activation (Supplementary Videos 1–3). Since the activation of Nurr1 by PGA1 can be stabilized by covalent binding, this modification can accumulate, allowing Nurr1 activation for a longer duration until

the protein is degraded by the proteasome system, as similarly proposed for covalent binding of ligands to PPAR γ ²⁴, suggesting that such ligands may have mechanistic advantages, previously referred to as the 'covalent advantage'⁴⁰.

Another interesting feature of our data is that PGE1 regulates Nurr1 by two distinct mechanisms (that is, via direct binding to Nurr1-LBD and to the EP2 receptor), while PGA1 works through direct binding to Nurr1-LBD only (Supplementary Fig. 16). In general agreement with our data, previous studies reported PGA1's neuroprotective effects using both in vitro cell culture and in vivo animal models^{41–43}. Our findings provide mechanistic insights into

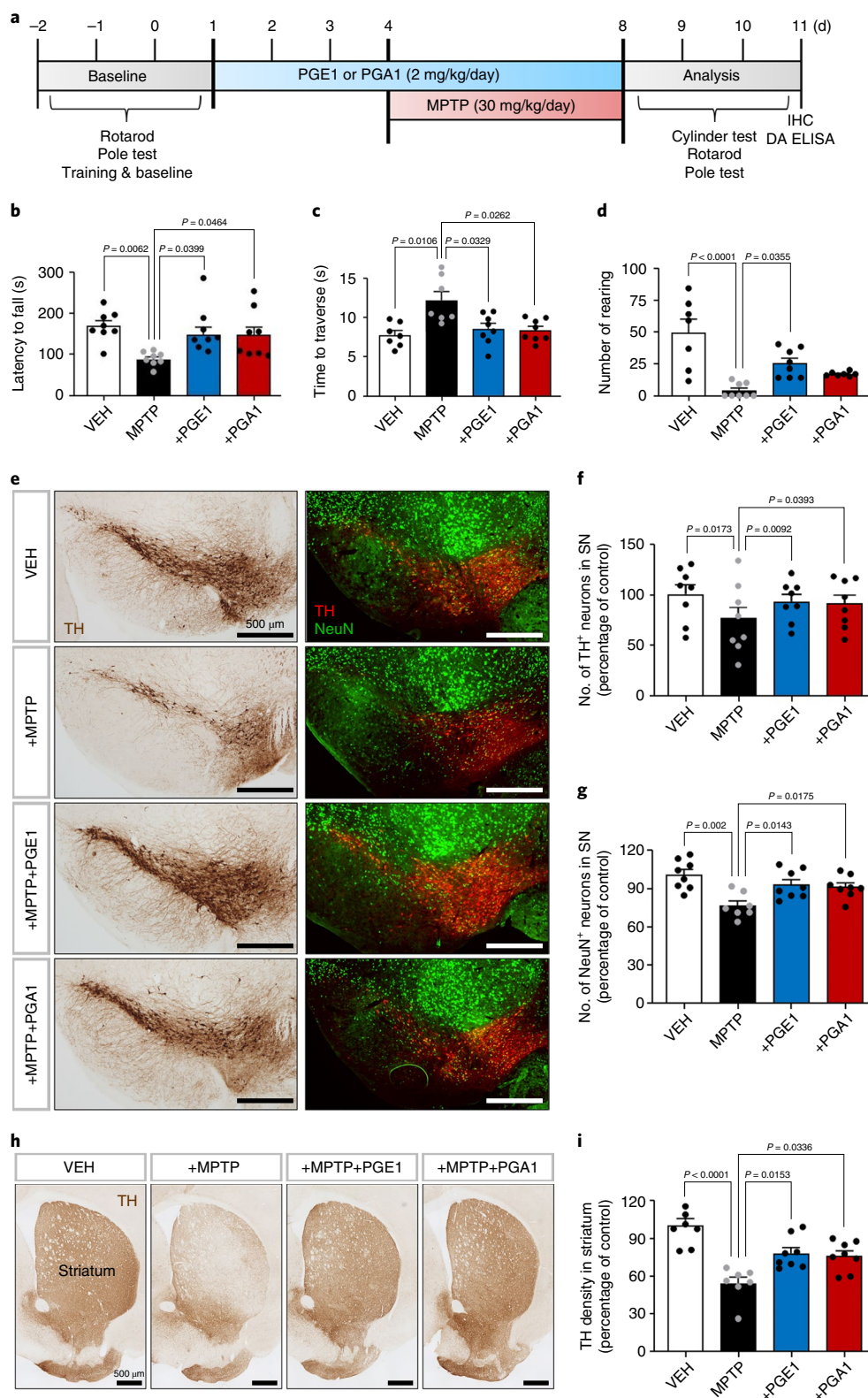


Fig. 6 | Neuroprotective effects of PGE1 and PGA1 in the MPTP-induced PD mouse model. a, Schematic representation of PGE1 and PGA1 administrations to MPTP-treated mice. PGE1 and PGA1 (2 mg kg^{-1}) were administered 3 d before subchronic MPTP regimen ($30 \text{ mg kg}^{-1} \text{d}^{-1}$, 5 d) and continued during MPTP administration until day 8. **b–d**, Motor behaviors were assessed on the days indicated in **a**; PGE1 and PGA1 treatments significantly rescue motor deficits on the rotarod latency to fall (**b**) and reduce time to traverse on a pole (**c**) compared to MPTP treatment: PGE1-treated mice recovered rearing numbers in the cylinder test (**d**). One-way ANOVA, Tukey's post hoc test; $n = 8$ per group. Data are mean \pm s.e.m. **e–i**, Immunohistochemical analyses of subchronic MPTP-treated mice after PGE1 and PGA1 administrations. The administration of PGE1 or PGA1 significantly rescues TH-positive DA neurons (**e,f**) and NeuN-positive neurons (**g**) in the SN and retains TH density (**h,i**) in the striatum compared to MPTP-treated mice. * $P < 0.05$, ** $P < 0.01$, *** $P < 0.001$, one-way ANOVA, Tukey's post hoc test; $n = 8$ per group. Data are mean \pm s.e.m.

the PGE1/PGA1-mediated pathways that regulate mDA neurons by functional modulation of Nurr1 through direct binding to its LBD and/or through GPCR (for example, EP2)-mediated activation. Since other NR4A members (that is, Nor1 and Nur77) share sequence homology with Nurr1, it is possible that PGE1/PGA1 could activate these NR4A members via direct binding to their LBDs. Our initial experiment indicated that PGE1/PGA1 preferably activate the transcription function of Nurr1 over Nor1 and Nur77 (Supplementary Fig. 17a). Furthermore, we found that PGE1/PGA1's chemical homologs such as PGE2 and PGE3 similarly activate Nurr1's transcriptional function (Supplementary Fig. 17b). Recently, a DA metabolite 5,6-dihydroxyindole was shown to bind and modulate the activity of Nurr1 (ref. 44). Therefore, these data suggest the possibility that a selective group of prostaglandins and other metabolites may serve as Nurr1 ligands.

A critical question is whether these native ligands can exert their biological function under physiological and/or pathophysiological conditions. In most of our cell-based analyses, relatively high concentrations of PGE1/PGA1 in the micromolar range (1–10 μ M) were required for activation of Nurr1's function. Similarly, other well-known endogenous ligands (for example, 15d-PGJ2 for PPAR γ , oxysterol for LXR α and DHA for RXR) also activated their reporter genes in the μ M ranges in cotransfection assays^{45,46} (also see Supplementary Fig. 2). Thus, although 15d-PGJ2 was identified as an endogenous ligand for PPAR γ , this finding was challenged because its intracellular concentration is below the levels required to induce PPAR γ 's biological effects⁴⁷. We speculated that higher concentrations of PGE1/PGA1 are required because cotransfection assays in cell lines are based on artificial and nonphysiological systems. Thus, we sought to test whether PGE1/PGA1 have a biological function under more physiological conditions using the rat primary mDA neuron-glia coculture system. Indeed, our data showed that both PGE1 and PGA1 exhibited prominent neuroprotective effects in the nanomolar range, suggesting that they can exert relevant function in physiological conditions. Taken together, while further studies are warranted, these data suggest the possibility that PGE1/PGA1 may represent bona fide endogenous ligands of Nurr1.

In sum, our results show that PGE1/PGA1 prominently stimulate Nurr1's transcriptional function via their direct binding to its LBD and/or PGE1's interaction with the EP2 receptor (Supplementary Fig. 16), protect mDA cells against neurotoxin-induced cytotoxicity, induce DA-related gene expression with upregulation of DA levels, and ameliorate motor deficits in a mouse model of PD in a neuroprotective manner. These structural and functional data shed new insights into the regulation of Nurr1's function by small molecule agonists, strongly suggesting that native and/or synthetic ligands of Nurr1 may be developed as a novel class of mechanism-based neuroprotective drugs for PD and other human disorders involving Nurr1 dysfunction.

Online content

Any Nature Research reporting summaries, source data, extended data, supplementary information, acknowledgements, peer review information; details of author contributions and competing interests; and statements of data and code availability are available at <https://doi.org/10.1038/s41589-020-0553-6>.

Received: 22 August 2019; Accepted: 22 April 2020;

Published online: 25 May 2020

References

- Mangelsdorf, D. J. et al. The nuclear receptor superfamily: the second decade. *Cell* **83**, 835–839 (1995).
- Evans, R. M. & Mangelsdorf, D. J. Nuclear receptors, RXR, and the big bang. *Cell* **157**, 255–266 (2014).
- Kliwer, S. A., Lehmann, J. M. & Willson, T. M. Orphan nuclear receptors: shifting endocrinology into reverse. *Science* **284**, 757–760 (1999).
- Kurakula, K., Koenis, D. S., van Tiel, C. M. & de Vries, C. J. NR4A nuclear receptors are orphans but not lonesome. *Biochim Biophys. Acta* **1843**, 2543–2555 (2014).
- Pearen, M. A. & Muscat, G. E. Minireview: nuclear hormone receptor 4A signaling: implications for metabolic disease. *Mol. Endocrinol.* **24**, 1891–1903 (2010).
- Zetterstrom, R. H. et al. Dopamine neuron agenesis in Nurr1-deficient mice. *Science* **276**, 248–250 (1997).
- Kadkhodaei, B. et al. Nurr1 is required for maintenance of maturing and adult midbrain dopamine neurons. *J. Neurosci.* **29**, 15923–15932 (2009).
- Saijo, K. et al. A Nurr1/CoREST pathway in microglia and astrocytes protects dopaminergic neurons from inflammation-induced death. *Cell* **137**, 47–59 (2009).
- Chu, Y. et al. Nurr1 in Parkinson's disease and related disorders. *J. Comp. Neurol.* **494**, 495–514 (2006).
- Moran, L. B. et al. Analysis of alpha-synuclein, dopamine and parkin pathways in neuropathologically confirmed Parkinsonian nigra. *Acta Neuropathol.* **113**, 253–263 (2007).
- Decressac, M., Volakakis, N., Bjorklund, A. & Perlmann, T. NURR1 in Parkinson disease—from pathogenesis to therapeutic potential. *Nat. Rev. Neurol.* **9**, 629–636 (2013).
- Kim, C. H., Leblanc, P. & Kim, K. S. 4-amino-7-chloroquinoline derivatives for treating Parkinson's disease: implications for drug discovery. *Expert Opin. Drug Discov.* **11**, 337–341 (2016).
- Kim, K. S. Toward neuroprotective treatments of Parkinson's disease. *Proc. Natl Acad. Sci. USA* **114**, 3795–3797 (2017).
- Wang, Z. et al. Structure and function of Nurr1 identifies a class of ligand-independent nuclear receptors. *Nature* **423**, 555–560 (2003).
- Kagaya, S. et al. Prostaglandin A2 acts as a transactivator for NOR1 (NR4A3) within the nuclear receptor superfamily. *Biol. Pharm. Bull.* **28**, 1603–1607 (2005).
- Lakshmi, S. P., Reddy, A. T., Banno, A. & Reddy, R. C. Molecular, chemical, and structural characterization of prostaglandin A2 as a novel agonist for Nur77. *Biochem. J.* **476**, 2757–2767 (2019).
- Vinayavekhin, N. & Saghatelian, A. Discovery of a protein-metabolite interaction between unsaturated fatty acids and the nuclear receptor Nur77 using a metabolomics approach. *J. Am. Chem. Soc.* **133**, 17168–17171 (2011).
- de Vera, I. M. et al. Identification of a binding site for unsaturated fatty acids in the orphan nuclear receptor Nurr1. *ACS Chem. Biol.* **11**, 1795–1799 (2016).
- de Vera, I. M. S. et al. Defining a canonical ligand-binding pocket in the orphan nuclear receptor Nurr1. *Structure* **27**, 66–77 e65 (2019).
- Chintharlapalli, S. et al. Activation of Nur77 by selected 1,1-bis(3'-indolyl)-1-(p-substituted phenyl)methanes induces apoptosis through nuclear pathways. *J. Biol. Chem.* **280**, 24903–24914 (2005).
- Zhan, Y. et al. Cytosporone B is an agonist for nuclear orphan receptor Nur77. *Nat. Chem. Biol.* **4**, 548–556 (2008).
- Kim, C. H. et al. Nuclear receptor Nurr1 agonists enhance its dual functions and improve behavioral deficits in an animal model of Parkinson's disease. *Proc. Natl Acad. Sci. USA* **112**, 8756–8761 (2015).
- Andersen, N. H. Dehydration of prostaglandins: study by spectroscopic method. *J. Lipid Res.* **10**, 320–325 (1969).
- Itoh, T. et al. Structural basis for the activation of PPARgamma by oxidized fatty acids. *Nat Struct. Mol. Biol.* **15**, 924–931 (2008).
- Codina, A. et al. Identification of a novel co-regulator interaction surface on the ligand binding domain of Nurr1 using NMR footprinting. *J. Biol. Chem.* **279**, 53338–53345 (2004).
- Aarnisalo, P., Kim, C. H., Lee, J. W. & Perlmann, T. Defining requirements for heterodimerization between the retinoid X receptor and the orphan nuclear receptor Nurr1. *J. Biol. Chem.* **277**, 35118–35123 (2002).
- Zhan, Y. Y. et al. The orphan nuclear receptor Nur77 regulates LKB1 localization and activates AMPK. *Nat. Chem. Biol.* **8**, 897–904 (2012).
- Li, L. et al. Impeding the interaction between Nur77 and p38 reduces LPS-induced inflammation. *Nat. Chem. Biol.* **11**, 339–346 (2015).
- Wang, W. J. et al. Orphan nuclear receptor TR3 acts in autophagic cell death via mitochondrial signaling pathway. *Nat. Chem. Biol.* **10**, 133–140 (2014).
- Wang, W. J. et al. Induction of autophagic death in cancer cells by agonizing TR3 and attenuating Akt2 activity. *Chem. Biol.* **22**, 1040–1051 (2015).
- Furuyashiki, T. & Narumiya, S. Stress responses: the contribution of prostaglandin E(2) and its receptors. *Nat. Rev. Endocrinol.* **7**, 163–175 (2011).
- Carrasco, E., Casper, D. & Werner, P. PGE(2) receptor EP1 renders dopaminergic neurons selectively vulnerable to low-level oxidative stress and direct PGE(2) neurotoxicity. *J. Neurosci. Res.* **85**, 3109–3117 (2007).
- Parga, J. A. et al. Prostaglandin EP2 receptors mediate mesenchymal stromal cell-neuroprotective effects on dopaminergic neurons. *Mol. Neurobiol.* **55**, 4763–4776 (2018).
- Xu, H. et al. The MDM2-binding region in the transactivation domain of p53 also acts as a Bcl-X(L)-binding motif. *Biochemistry* **48**, 12159–12168 (2009).

35. Becker, W., Bhattiprolu, K. C., Gubensak, N. & Zangger, K. Investigating protein-ligand interactions by solution nuclear magnetic resonance spectroscopy. *Chem. Phys. Chem.* **19**, 895–906 (2018).
36. Choi, H. K., Won, L., Roback, J. D., Wainer, B. H. & Heller, A. Specific modulation of dopamine expression in neuronal hybrid cells by primary cells from different brain regions. *Proc. Natl Acad. Sci. USA* **89**, 8943–8947 (1992).
37. Gao, L., Zhou, W., Symmes, B. & Freed, C. R. Re-cloning the N27 dopamine cell line to improve a cell culture model of Parkinson's disease. *PLoS ONE* **11**, e0160847 (2016).
38. af Forselles, K. J. et al. In vitro and in vivo characterization of PF-04418948, a novel, potent and selective prostaglandin EP(2) receptor antagonist. *Br. J. Pharmacol.* **164**, 1847–1856 (2011).
39. Bergstroem, S. & Samuelsson, B. Prostaglandins. *Annu. Rev. Biochem.* **34**, 101–108 (1965).
40. Higdon, A., Diers, A. R., Oh, J. Y., Landar, A. & Darley-USmar, V. M. Cell signalling by reactive lipid species: new concepts and molecular mechanisms. *Biochem. J.* **442**, 453–464 (2012).
41. Qin, Z. H. et al. Prostaglandin A(1) protects striatal neurons against excitotoxic injury in rat striatum. *J. Pharmacol. Exp. Ther.* **297**, 78–87 (2001).
42. Wang, X. et al. Prostaglandin A1 inhibits rotenone-induced apoptosis in SH-SY5Y cells. *J. Neurochem.* **83**, 1094–1102 (2002).
43. Zhang, H. L. et al. Neuroprotective effects of prostaglandin A1 in animal models of focal ischemia. *Brain Res.* **1039**, 203–206 (2005).
44. Bruning, J. M. et al. Covalent modification and regulation of the nuclear receptor nurr1 by a dopamine metabolite. *Cell Chem. Biol.* **26**, 674–685 e676 (2019).
45. de Urquiza, A. M. et al. Docosahexaenoic acid, a ligand for the retinoid X receptor in mouse brain. *Science* **290**, 2140–2144 (2000).
46. Janowski, B. A., Willy, P. J., Devi, T. R., Falck, J. R. & Mangelsdorf, D. J. An oxysterol signalling pathway mediated by the nuclear receptor LXR alpha. *Nature* **383**, 728–731 (1996).
47. Powell, W. S. 15-Deoxy-delta12,14-PGJ2: endogenous PPARgamma ligand or minor eicosanoid degradation product? *J. Clin. Invest.* **112**, 828–830 (2003).

Publisher's note Springer Nature remains neutral with regard to jurisdictional claims in published maps and institutional affiliations.

© The Author(s), under exclusive licence to Springer Nature America, Inc. 2020

Methods

Cell culture and luciferase assay. Human neuroblastoma SK-N-BE(2)C cells were grown in Dulbecco's modified Eagle's medium (DMEM) supplemented with 10% fetal bovine serum (FBS) and antibiotics (100 U ml⁻¹ penicillin and 100 µg ml⁻¹ streptomycin). The murine MN9D cell line was kindly provided by M. Zigmond and J. Jaumotte from the University of Pittsburgh, and grown in the same medium as SK-N-BE(2)C cells. C. Freed from the University of Colorado School of Medicine kindly provided the rat N27-A cell line that was cultured in RPMI 1640 medium supplemented with 10% FBS and antibiotics. One day before transfection, cells were plated onto 48-well plates without antibiotics and then transfected with plasmids (for Nurr1-LBD, pGAL-Nurr1(LBD), p8xUAS-Luc and pRSV-β-gal; for full-length Nurr1, pCMV fNurr1, p4xNL3-Luc, pRSV-β-gal) using lipofectamine reagent (Thermo Fisher Scientific)²². Twenty-four hours after transfection, cells were lysed with lysis buffer (25 mM Tris-phosphate (pH 7.8), 2 mM DTT, 2 mM CDTA (1,2-diaminocyclohexane-N,N,N',N'-tetraacetic acid), 10% glycerol and 1% Triton X-100). Firefly luciferase activity was measured using a luminometer plate reader (SpectraMax, Molecular Device). Transfection efficiency was normalized using β-galactosidase activity.

Plasmid constructs and chemicals. All plasmids were described previously²². For chemicals, thromboxane B2 (no. 19030), lipoxin A4 (no. 90410), leukotriene B4 (no. 20110), PGD1 (no. 12000), PGD2 (no. 12010), PGF1α (no. 15010), PGF2α (no. 16010), 8-iso PGF2α (no. 16395), 20-hydroxy PGF2α (no. 16950), PGE1 (no. 13010), PGE2 (no. 14010), PGE3 (no. 14990), PGA1 (no. 10010), 15d-PGJ2 (no. 18570), 9-*cis*-retinoic acid (no. 14587), 27-hydroxycholesterol (no. 14791), cortisol (no. 16063) and MPP⁺ iodide (no. 16958) were all purchased from Cayman Chemical. MPTP hydrochloride (M0896) and lipopolysaccharides (LPS, L7770) were purchased from Sigma-Aldrich.

Tissue preparation and active compounds isolation. BALB/c mice (8 weeks, male; Jackson Laboratories) were perfused with PBS and then organs were placed in 20 mM sodium acetate (pH 5.2) buffer, cut into small pieces, and homogenized by sonication. Tissues were incubated at 37 °C for 2 h and centrifuged, then the supernatants were boiled for 5 min and centrifuged. After cooling on ice, a double volume of acetone was added to the supernatant. The acetone-treated extract was centrifuged to remove the precipitated proteins and evaporated to remove the acetone. The dried extracts were reconstituted in 20 mM sodium acetate buffer and ultrafiltered through a Centricon-3 concentrator. Supernatants, retentates and filtrates prepared at each step were assayed for the presence of any Nurr1-enhancing activities using our established cell-based assays²². For preparative high-performance liquid chromatography (prep-HPLC), we used a Hitachi prep-HPLC equipped with a C18 reversed-phase column (YMC-Pack Pro C18, 250 × 4.6 mm²) and a photodiode array detector (ultraviolet wavelength 200–500 nm) to separate active compounds from the extract solution. The mobile phases consisted of 5% acetonitrile in water (A) and 100% acetonitrile (B) and the gradient elution was programmed as follows: 0–65 min, gradually increased from 0 to 100% B and 60–70 min, sharply reduced to 100% A.

Ultra-performance liquid chromatography–quadrupole time of flight–tandem MS (UPLC–qTOF–MS/MS). UPLC–qTOF–MS/MS analysis was performed using a Waters Micromass Q-TOF Premier with UPLC Acquity system (Waters Corp.) equipped with a UPLC mass spectrometer. The UPLC system was equipped with an Acquity UPLC BEH C18 column (100 × 2.1 mm², 1.7-µm particle size; Waters Corp.). The mobile phase consisted of 0.1% (v/v) formic acid in water (A) and 0.1% (v/v) formic acid in acetonitrile (B). The solvent gradient profile consisted of the following: 5% B for 1 min, gradually increased to 100% B over 9 min and held at 100% B for 1 min, then decreased to 5% B for 1 min, and maintained for 1 min. Total run time was 13 min. The injection volume was 5 µl, and the column temperature and flow rate were set at 37 °C and 0.3 ml min⁻¹, respectively. An *m/z* 100–1,000 scale was designated with the ESI negative and positive modes. The operating parameters were as follows: ion source temperature, 100 °C; desolvation gas flow, 650 l h⁻¹; capillary voltage, 2.5 kV and cone voltage, 50 V. The V mode was used for the mass spectrometer and data were collected in the centroid mode with a scan accumulation 0.2 s. Following UPLC analysis, the assignment of metabolites contributing to active components were performed by elemental composition analysis software with the calculated mass, mass tolerance (mDa and ppm), double bond equivalents (DBEs) and iFit algorithm implemented in the Mass Lynx and were putatively identified using the Human Metabolome Database (HMDB, <http://www.hmdb.ca>).

Chromatin immunoprecipitation (ChIP). PC12 cells were cross-linked using 1% formaldehyde for 30 min. Cross-linked cells were sonicated according to the manufacturer's instruction (Active Motif). Thereafter, DNA–protein complexes in the lysates were immunoprecipitated using anti-Nurr1, anti-SRC1, anti-SRC3 or control normal IgG. After precipitation of the immunocomplex with protein G-agarose, isolated DNAs were used as PCR template with specific primers containing the TH promoter target region. The specific primers used for amplification of the TH promoter were as follows: 5'-TCC TTA GAG ATC CTG TTT CC-3' and 5'-TCA GCT GGT CCC CAT GTA AG-3'.

Protein expression, purification, crystallization and structure determination.

The human Nurr1-LBD was prepared as previously described²². The purified Nurr1-LBD^{328–598} in 50 mM Tris (pH 8.0) and 150 mM NaCl was concentrated to 10 mg ml⁻¹ and incubated overnight with Prostaglandin A1 (PGA1) (SantaCruz Biotechnology) at a 1:4 molar ratio for crystallization. Crystals were obtained using hanging drop vapor diffusion with 20% PEG 3350, 0.1 M MES (pH 5.5) and 0.2 M MgCl₂. X-ray data collection was carried out at 100 K using a wavelength of 1.0000 Å on beamline X06DA of the Swiss Light Source (Villigen), with 20% ethylene glycol as the cryo protectant supplemented to the reservoir solution. The best data was obtained from a Nurr1-LBD-PGA1 cocrystal that diffracted to 2.05 Å. Data was indexed, integrated, merged and scaled using IMOSFLM⁴⁸ and SCALA⁴⁹ from CCP4 suite of programs⁵⁰. The crystal belonged to the orthorhombic space group P2₁2₁2, with two molecules in the asymmetric unit. Molecular replacement using PHASER⁵¹ with apo Nurr1-LBD structure (Protein Data Bank (PDB) ID 1OVL) was used as the search model. REFMAC⁵² and COOT⁵³ were used for refinement and map fitting, respectively, while the PyMOL Molecular Graphics System (DeLano Scientific) was used to generate the figures and the movie was generated using Chimera software⁵⁴. The electron density indicated reorientation of the H12 helix, which was traced manually using COOT. The electron density for PGA1 was unequivocally observed packed mainly by H12, H4 and H11 helices in chain B, which was also validated by calculating an omit map (Supplementary Fig. 18) using PHENIX software⁵⁵. The electron density for few atoms at the flexible carboxyl end of PGA1 bound to chain A was missing at 1σ cut-off of the 2Fo-Fc map. Therefore, the structure analysis and representations shown here have been confined to chain B alone. Water molecules were manually picked from the Fo-Fc and 2Fo-Fc electron density map contoured at 3.0 and 1.0σ cut-offs, respectively. Two PEG molecules and a magnesium ion, from the crystallization solution, trapped in the monomer interfaces were also observed during map fitting. The Ramachandran statistics revealed that 99.1 and 0.9% residues in the preferred and allowed regions, respectively. Data collection and refinement statistics are summarized in Supplementary Table 2. In addition, cocrystals of Nurr1-LBD in complex with PGE1 (SantaCruz Biotechnology) were also obtained under similar conditions, and the best crystal diffracted to 2.4 Å at 100 K using a wavelength of 1 Å on beamline X10SA at the Swiss Light Source (Villigen). The structure revealed that the molecule had been dehydrated to PGA1 in the bound form, as evidenced from the covalent bonding with atom C11 (Extended Data Fig. 4a). This could be a reflection of the conditions used for crystallization (Extended Data Fig. 4b).

NMR data collection and analysis. Uniformly ¹⁵N-labeled Nurr1-LBD^{356–598} (0.2 mM) was prepared in 20 mM sodium phosphate (pH 7.5) buffer containing 50 mM NaCl, 0.01% NaN₃ in 90% H₂O/10% D₂O. Molecular interaction between Nurr1-LBD and PGE1/A1 was studied by two-dimensional ¹H-¹⁵N HSQC NMR spectroscopy using uniformly ¹⁵N-labeled Nurr1-LBD (0.2 mM) on a Bruker Avance II 700 MHz spectrometer. CSPs were analyzed, as previously described²². The binding sites of PGE1/PGA1 were mapped on the crystal structure of Nurr1-LBD (PDB 1OVL) after determining the CSPs and resonance line broadening following the addition of PGE1/PGA1 against the spectrum of the free protein. Analysis of selected peaks for *K_D* and *k_{off}* values, were performed using the software tool TiTan (TiTitration ANalysis)⁵⁶. A series of titration points of 1:0.25, 1:0.5, 1:1, 1:2, 1:5 and 1:10 was set up for PGA1 while Nurr1-LBD:PGE1 was 1:4 and 1:10. From the software, the HSQC pulse program and two-state binding model were selected. Next, the spin systems were specified by selecting regions of interest for selected residues L559, Q571, K590, F592 and T595. The parameters for the first spectrum (apo) was held constant for fitting of subsequent spectra (bound). Following a satisfactory fit, bootstrap error analysis of 100 replicas was performed to determine covariances and errors in parameters.

Top-down MS. Nurr1-LBD at ~300 µM prepared in 0.1% formic acid in water was analyzed using a Dionex UltiMate 3000 UPLC coupled to a linear quadrupole ion trap-Fourier transform Ultra apparatus (LTQ-FT Ultra, Thermo Fisher Scientific). A protein solution (5 µl) was injected directly into the detector carried by 0.1% formic acid in water at 500 µl min⁻¹. Online ionization was performed using a Michrom CaptiveSpray ion source (Bruker-Michrom Inc.) at an electrospray potential of 1.5 kV and capillary temperature of 200 °C. Data acquisition was conducted in profile and positive mode (600–1,600 *m/z* range). MS data was acquired for 60 min in the Fourier-transform ion cyclotron resonance MS cell at a resolution of 100,000 (at 400 *m/z*) and maximum injection time of 500 ms using the Xcalibur v.2.0 SR2 (Thermo Fisher Scientific). The automatic gain control target for Fourier-transform ion cyclotron resonance MS was set to 5.0 × 10³. For each scan, 100 microscans were averaged. The Xtract software was used for Peak deconvolution (Thermo Fisher Scientific) with a S/N threshold of five and a fit factor of 44%. A similar protocol was adopted for Nurr1-LBD, in 50 mM Tris pH 8.0 and 150 mM NaCl, incubated with PGE1 and PGA1 overnight at 1:1.5 molar ratio followed by buffer exchange to 0.1% formic acid in water before injection.

Western blot and co-IP. Protein lysates were prepared in RIPA cell lysis buffer (Sigma-Aldrich) containing a protease inhibitor mixture (Roche). Equal amounts

of protein samples were subjected to electrophoresis and then transferred to a PVDF membrane. After blocking the membrane for 1 h with a PBS-T buffer (137 mM NaCl, 2.7 mM KCl, 10 mM Na₂HPO₄, 1.8 mM KH₂PO₄, 0.1% Tween 20) containing 2% skimmed milk and 0.1% horse serum (HS) it was incubated with primary antibodies against c-myc (Clone 9E10, Roche Diagnostics), Nurr1 (prepared in our laboratory)³⁷ and β -actin (Abcam) overnight at 4 °C. After incubation with secondary antibody for 1 h, immunoblot detection was achieved using the Novex ECL HRP Chemiluminescent substrate. Band intensities were determined using ImageJ software (v.2.0.0-rc-69/1.52n; NIH) and then normalized against β -actin values. For co-IP, protein samples were prepared from collected cells and each protein sample (40 μ g) was incubated with mouse anti-c-myc (1:1,000; Sigma-Aldrich) and GammaBind G Sepharose slurry (Sigma-Aldrich) for IP overnight at 4 °C with gentle rotation. After washing, samples were subjected to immunoblot against Nurr1 (1:1,000).

Quantitative real-time PCR (qRT-PCR). Total RNA was isolated from cells using GeneJET RNA Purification Kits (Thermo Fisher Scientific) and complementary DNA was synthesized using Invitrogen Superscript cDNA Synthesis Kits (Thermo Fisher Scientific) following the manufacturer's protocol. The following primers were used: TH, forward 5'-CAA GGT TCC CTG GTT CCC AA-3', reverse 5'-CTT CAG CGT GGC GTA TAC CT-3'; VMAAT2, forward 5'-ATG TGT TCC CGA AAG TGG CA-3', reverse 5'-AAG TTG GGA GCG ATG AGT CC-3'; DAT, forward 5'-GTC ACC AAC GGT GGC ATC TA-3', reverse 5'-TAG GCT CCA TAG TGT GGG GG-3'; AADC, forward 5'-CAC GGC TAG CTC ATA CCC AG-3', reverse 5'-GCT CTT CCA GCC AAA AAG GC-3'; Pitx3, forward 5'-GCT ACC CTG ACA TGA GCA CC-3', reverse 5'-TAC ACC TCC TCG TAG GGT GG-3'; c-RET, forward 5'-TGC TGC TCT GGG AGA TTG TG-3', reverse 5'-AAC ACT GGC CTC TTG TCT GG-3'; glyceraldehyde-3-phosphate dehydrogenase (GAPDH), forward 5'-GAA GGT CGG TGT GAA CGG AT-3', reverse 5'-TTC CCA TT C TCG GCC TTG AC-3'. Gene expression levels were quantified by the $2^{-\Delta\Delta CT}$ method (C_t of target gene, C_t of GAPDH).

Binding and competition assays. Saturation and competition assays were performed as described previously²². Briefly, 0.2 μ M of Nurr1-LBD or 0.38 μ M of EP2 (Cloud-Clone Corp.) and 3.9–1,000 nM of [³H]-PGE1 or [³H]-PGA1 (Moravik Biochemicals Inc.) were incubated in binding buffer (20 mM sodium acetate (pH 5.2)) at 4 °C overnight. GF/B filters (Brandel Inc.) wetted with binding buffer were placed on a 48-place Cell Harvester and 1 ml of assay mixtures were applied on the surface of the filter through suctioning. After washing with binding buffer four times, filters were dried and soaked in 5 ml of ScintiVerse (Thermo Fisher Scientific). Radioactivity was determined using a Beckman LS6500 Liquid Scintillation Counter (Beckman Coulter). For competition assay, proteins (Nurr1-LBD (0.2 μ M) or EP2 (0.38 μ M)) and tritium-labeled ligands ([³H]-PGE1 (500 nM) or [³H]-PGA1 (1,000 nM)) were simultaneously incubated with various concentrations of unlabeled competitors (PGE1, PGA1, misoprostol, retinoic acid or 15d-PGJ2) in binding buffer at 4 °C overnight. Assay mixtures were applied to GF/B filters and counted as described above. Nonspecific binding was determined in the presence of a 1,000-fold molar excess of unlabeled PGE1 or PGA1. Specific binding was calculated as the difference of total and nonspecific binding. The competition assay values were transformed as a percentage of inhibition relative to 0 nM of competitors. All graphs, K_d and B_{max} values were generated using the nonlinear regression program in GraphPad Prism v.8.0.2.

ELISA. The concentrations of PGE1, PGA1 and endogenous DA in cultured cells and brain tissue extracts were determined using ELISA Kits according to the manufacturer's instructions: mouse PGE1 (Enzo Life Sciences, catalog no. ADI-900-005), mouse PGA1 (MyBiosource, catalog no. MBS9346924) and mouse DA (MyBiosource, catalog no. MBS732020).

Stereotaxic injection. Male C57BL/6 mice (12 weeks, 25–30 g) were anesthetized using a gaseous mixture of O₂ and isoflurane (induction 2.5%; maintenance 1.5%), then placed on a Kopf stereotaxic apparatus (David Kopf Instruments). Mice were bilaterally injected with 2 μ l of VEH or PGE1/PGA1 into the SN pars compacta (SNpc) according to the following coordinates: –3.3 anterior–posterior, \pm 1.5 mediolateral, and –4.3 dorsoventral. Stereotaxic injection was performed using a 10 μ l Hamilton syringe (Hamilton) with a 30-s gauge-beveled steel needle, at a rate of 0.4 μ l min⁻¹. All mice were killed 1 d after injection and brains were regionally dissected for biochemical analysis or perfused for immunohistochemical analysis. For injection, PGE1/PGA1 (50 mg ml⁻¹ in ethanol) was freshly diluted before administration to a final concentration of 1 mg ml⁻¹ in PBS, and then VEH (2% ethanol in PBS) or 2 μ g ml⁻¹ PGE1/PGA1 was administered to each side.

Nurr1 overexpression and knockdown. Human Nurr1 cloned into pcDNA3.1 vector was used for overexpression in cells. For Nurr1 knockdown, scrambled short-hairpin RNA (no. RHS4346) and shRNA (V3LHS_411033, TCTTCTGAACAACAACTG) were purchased from GE Dharmacon (Lafayette). Nurr1 expression levels from knockdown samples were assessed by rtPCR with reverse transcription and western blot.

Cellular oxidative stress and cytotoxicity. Cellular oxidative stress was fluorometrically monitored using the fluorescent probe, DCFH-DA (Sigma-Aldrich). DCFH-DA, diluted to a final concentration of 10 μ M with DMEM, was added to SK-N-BE(2)C cells followed by incubation at 37 °C for 20 min. DCF fluorescence images were acquired using a fluorescence microscope (Olympus Corporation). The intensity of fluorescence signals was measured using ImageJ software. Cytotoxicity was quantified by measuring lactate dehydrogenase (LDH) release into the culture medium using an LDH cytotoxicity detection kit (Roche) according to the manufacturer's instructions. Absorbance was measured with a microplate reader (Synergy HT, Bio-Tek) at 490 nm. LDH release is represented as the percentage of cytotoxicity calculated according to the manufacturer's instructions. To determine protective effect of PGE1/PGA1 on MPP⁺, cells were pretreated with PGE1 or PGA1 for 24 h, then incubated with MPP⁺ with or without PGE1/PGA1. Oxidative stress level and cytotoxicity were measured after 24 h exposure to MPP⁺.

3-(4,5-Dimethylthiazol-2-yl)-2,5-diphenyltetrazolium bromide (MTT) cell viability assay. Determination of cell viability using MTT was performed as previously described³⁸. Briefly, cells were incubated with 15 μ l of MTT (Sigma-Aldrich) solution (5 mg ml⁻¹ in PBS) for 3.5 h. MTT crystals were dissolved in 150 μ l of MTT solvent (4 mM HCl and 0.1% Nonidet P-40 in isopropanol) and the generated amount of blue formazan was determined spectrophotometrically at 570 nm.

Primary mDA neuron-glia coculture. Primary mDA neuron-glia coculture was prepared from E14 rat embryos (Fisher 344; Charles River Laboratories) as previously described³⁹. Briefly, dissociated ventral mesencephalic tissues were plated onto coverslips precoated with 20 μ g ml⁻¹ poly-D-lysine (Sigma-Aldrich) at a density of 2.5×10^5 cells cm⁻² in neuron-glia media (NG media, minimum essential medium supplemented with 10% heat-inactivated FBS, 10% heat-inactivated HS, nonessential amino acids, 1 mM sodium pyruvate, 2 mM L-glutamine, 0.1% D-glucose and antibiotics). On day 7, cells were pretreated with PGE1 or PGA1 30 min before MPP⁺ (0.3 μ M) or LPS (15 ng ml⁻¹) treatment and then analyzed by immunocytochemistry 7 d after treatments (14 d in vitro).

Immunocytochemistry. Cells were fixed with 4% formaldehyde for 10 min, and then washed three times with PBS. After blocking (3% bovine serum albumin (BSA) and 0.3% Triton X-100) for 1 h, cells were incubated overnight at 4 °C with rabbit anti-TH (1:1,000; Cctalog no. P40101, Pel Freez) and goat anti-iba-1 (1:500; catalog no. ab5076, Abcam). Cells were then incubated for 1 h at room temperature with Alexa Fluor 568-conjugated donkey anti-rabbit IgG and Alexa Fluor 488-conjugated donkey anti-goat IgG (Thermo Fisher Scientific). Fluorescence images were acquired using a KEYENCE microscope (BZ-X800; KEYENCE).

Acute and subchronic MPTP-Induced animal experiments. Animal care and handling was carried out according to guidelines issued by McLean Hospital's Institutional Animal Care and Use Committee and followed National Institutes of Health guidelines. We have complied with all relevant ethical regulations. Male C57BL/6 mice (8–10 weeks, 25–30 g; Jackson Laboratory) were used and they were provided with free access to food and water under a 12 h light/dark cycle.

Mice were randomly distributed into four groups including VEH, MPTP, MPTP + PGE1 and MPTP + PGA1 ($n=8$ for each group). Mice initially received VEH, PGE1 or PGA1 injections intraperitoneally (i.p.) 3 d before MPTP injection. PGE1 and PGA1 (10 mg ml⁻¹ in ethanol) was freshly diluted before every administration to a final concentration of 0.2 mg ml⁻¹ in PBS, then VEH (2% ethanol in PBS) or PGE1/PGA1 (2 mg kg⁻¹ d⁻¹) was administered to each group during pre- and posttreatment period. For acute MPTP regimen (Supplementary Fig. 14), mice received saline or MPTP (18 mg kg⁻¹, Sigma-Aldrich) four times (i.p.) at 2 h intervals on the fourth day of PGE1/PGA1 injection. For the subchronic MPTP regimen (Fig. 6), MPTP was administered as 30 mg kg⁻¹ (i.p.) for 5 d. Post-treatments with PGE1 or PGA1 were continued for 5 d. Behavior tests were performed on the following days as the assessor- and observer-blinded trial, and all mice were killed for immunohistochemistry.

Animal behaviors. Rotarod. Mice were pretrained on an automated five-lane rotarod unit (10 r.p.m., 3 min) for 3 d before MPTP injection. After 2 d of pretraining, baseline was determined at 10 r.p.m. for 90 s. Rotarod measurements were performed using an accelerating protocol, accelerated smoothly from 2 to 30 r.p.m. for 5 min. Time on the rod was measured automatically by placing a trip switch under the floor beneath the rotating drum.

Pole test. Mice were placed head-upward on the top of a vertical metal rod wrapped with tape (height, 80 cm, diameter, 12 mm). Three days before MPTP injection, mice were trained to descend the pole once per day. The total descent time was recorded for analysis.

Cylinder test. Mice were placed in a transparent plastic cylinder (height, 15.5 cm, diameter, 12.7 cm) with a mirror behind it. Spontaneous activity was measured as counting the number of rearing events over a 3 min period. A rear was counted

when the mouse made a vertical movement with both forelimbs off the floor and touched the wall of the cylinder.

Immunohistochemistry. Brain sections were incubated in blocking solution (3% BSA and 0.3% Triton X-100 in PBS) for 1 h, followed by incubation with mouse anti-TH (EMD Millipore) for overnight at 4 °C. DAB staining was performed according to the manufacturer's instruction (Vector Laboratories). Images were acquired using an optical light microscope (Carl Zeiss). TH immunoreactivity was measured as the number of TH-positive neurons in the SN and as an optical density of TH-containing fibers in the striatum using ImageJ software.

Experimental design and statistical analysis. We randomly allocated all samples and animals without prejudice. All attempts for each experiment were replicated at least three times. All results are shown as mean \pm s.e.m. Unpaired two-tailed Student *t*-test or Welch's *t*-test was used to determine the statistical differences between two means. A one-way analysis of variance (ANOVA) with Tukey's post hoc analysis was used to conduct multiple comparisons of the means. Statistical significance was accepted for *P* values of <0.05 (*), 0.01 (**), or 0.001 (***)

Reporting Summary. Further information on research design is available in the Nature Research Reporting Summary linked to this article.

Data availability

The PDB accession code for the coordinates and structure factors of Nurr1-LBD in complex with PGA1 is PDB 5Y41. Source data for Figs. 1–3 and Extended Data Figs. 1–9 are presented with the paper.

References

- Battye, T. G., Kontogiannis, L., Johnson, O., Powell, H. R. & Leslie, A. G. iMOSFLM: a new graphical interface for diffraction-image processing with MOSFLM. *Acta Crystallogr. D.* **67**, 271–281 (2011).
- Evans, P. Scaling and assessment of data quality. *Acta Crystallogr. D.* **62**, 72–82 (2006).
- Winn, M. D. et al. Overview of the CCP4 suite and current developments. *Acta Crystallogr. D.* **67**, 235–242 (2011).
- McCoy, A. J. et al. Phaser crystallographic software. *J. Appl. Crystallogr.* **40**, 658–674 (2007).
- Murshudov, G. N. et al. REFMAC5 for the refinement of macromolecular crystal structures. *Acta Crystallogr. D.* **67**, 355–367 (2011).
- Emsley, P. & Cowtan, K. Coot: model-building tools for molecular graphics. *Acta Crystallogr. D.* **60**, 2126–2132 (2004).
- Pettersen, E. F. et al. UCSF Chimera—a visualization system for exploratory research and analysis. *J. Comput. Chem.* **25**, 1605–1612 (2004).
- Adams, P. D. et al. PHENIX: a comprehensive Python-based system for macromolecular structure solution. *Acta Crystallogr. D.* **66**, 213–221 (2010).
- Waudby, C. A., Ramos, A., Cabrita, L. D. & Christodoulou, J. Two-dimensional NMR lineshape analysis. *Sci. Rep.* **6**, 24826 (2016).
- Leblanc, P. et al. Production of Nurr-1 specific polyclonal antibodies free of cross-reactivity against its close homologs, Nor1 and Nur77. *J. Vis. Exp.* **102**, e52963 (2015).
- Kim, W. et al. miR-126 contributes to Parkinson's disease by dysregulating the insulin-like growth factor/phosphoinositide 3-kinase signaling. *Neurobiol. Aging* **35**, 1712–1721 (2014).
- Chen, S. H., Oyarzabal, E. A. & Hong, J. S. Preparation of rodent primary cultures for neuron-glia, mixed glia, enriched microglia, and reconstituted cultures with microglia. *Methods Mol. Biol.* **1041**, 231–240 (2013).

Acknowledgements

We thank various members of the molecular neurobiology laboratory past and present who participated in the project. In particular, we thank B.-S. Han, H.-Y. Jung, J. Lee and J. Sung Koh for technical assistance. We also acknowledge the contribution of the scientists and staff on the PXII and PXIII (Paul Scherrer Institute, Switzerland) beamlines for their expert assistance during crystal data collection. This work was supported by NIH grant nos. NS070577 and NS084869 (to K.-S.K.), NRF-2018M3A9B5023055 grant (to C.-H.K.), Ministry of Education Singapore AcRF Tier 2 Grant (no. ARC55/16) and Tang Tieng See Advancement Fund (to H.S.Y.), and National Medical Research Council, Singapore (grant no. TCR/013-NNI/2014; to K.L.L. and H.S.Y.).

Author contributions

K.-S.K. and H.S.Y. initiated and supervised the project. S.R., Y.J., C.H.K. and W.K. were responsible for the overall design and performance of experiments. S.R., H.T.T., H.Y., C.K., A.S., J.L., J.Y.Y., S.B., H.Y., C.K., X.L., G.G. and K.L.L. performed and analyzed structural studies. Y.J., C.H.K., W.K., J.J., B.S., M.F., Y.K., D.H., H.M.P., S.F.O. and C.H.L. performed and analyzed functional and biological studies. K.-S.K., H.S.Y., S.R., Y.J., C.H.K., W.K. and G.A.P. analyzed the data and wrote the paper. All authors contributed to the discussion and final approval of the paper.

Competing interests

H.S.Y. is a nonexecutive director of Lifex Biolabs. The remaining authors have no competing interests to disclose.

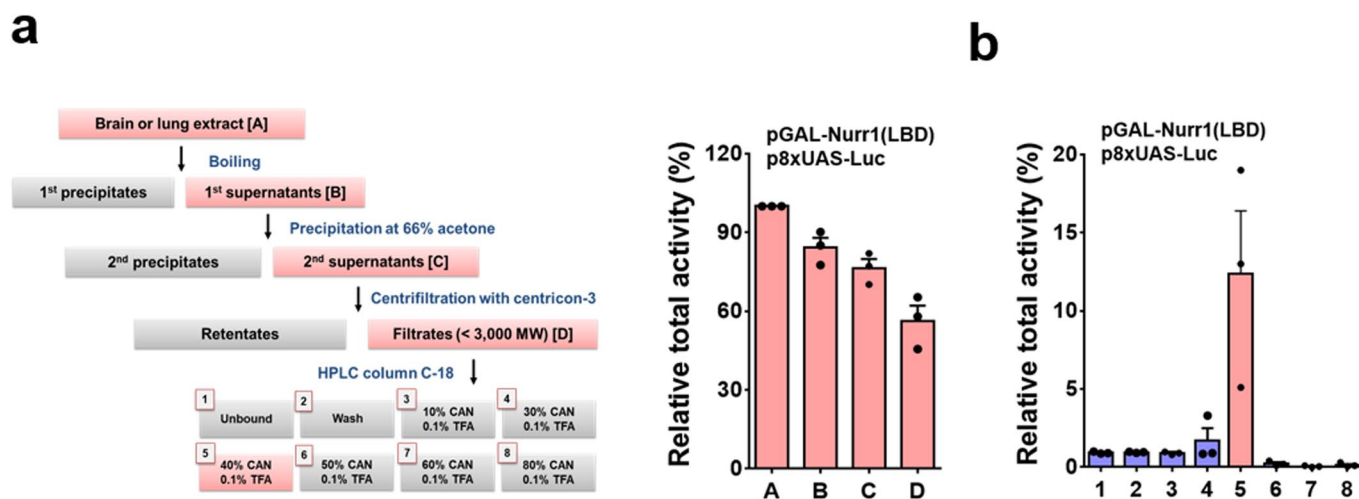
Additional information

Extended data is available for this paper at <https://doi.org/10.1038/s41589-020-0553-6>.

Supplementary information is available for this paper at <https://doi.org/10.1038/s41589-020-0553-6>.

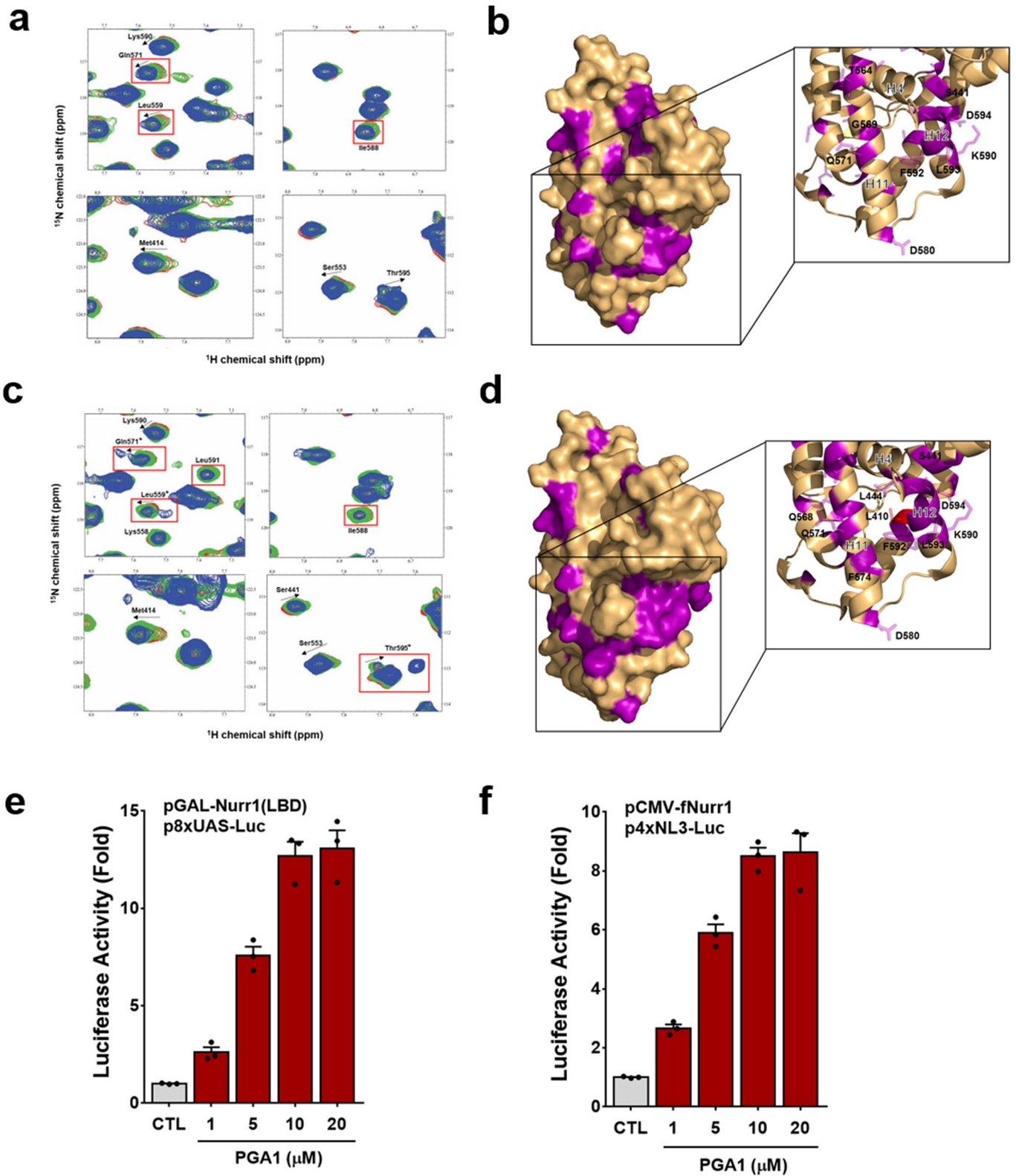
Correspondence and requests for materials should be addressed to H.S.Y. or K.-S.K.

Reprints and permissions information is available at www.nature.com/reprints.



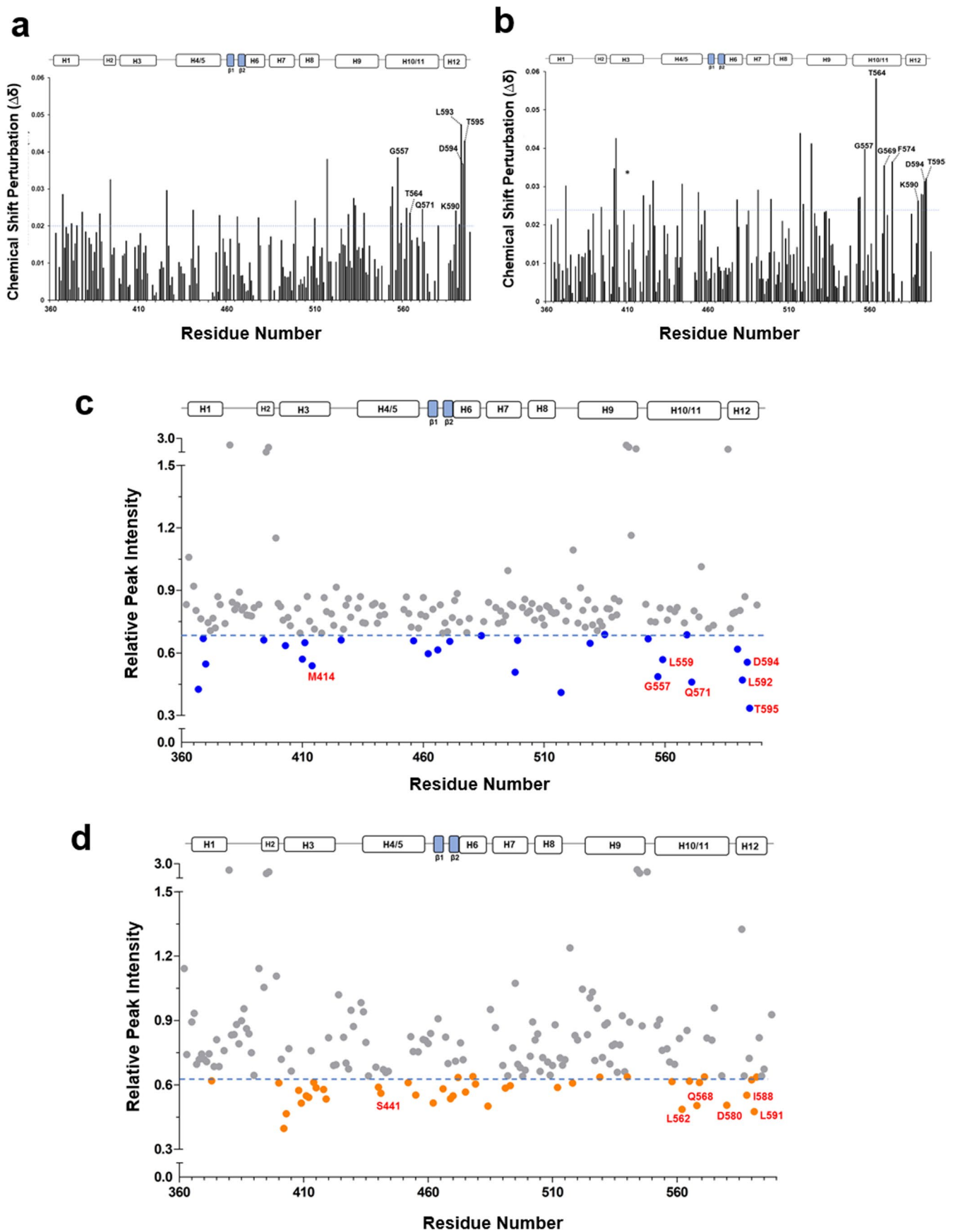
Tentative metabolites	Molecular weight	HMDB Formula	HMDB ID	Tentative metabolites	Molecular weight	HMDB Formula	HMDB ID
Thromboxane B2	370.48	C ₂₀ H ₃₄ O ₆	03252	Prostaglandin F2α (PGF2α)	354.48	C ₂₀ H ₃₄ O ₅	01139
13,14-Dihydro-lipoxin A4 (lipoxin A4)	354.5	C ₂₀ H ₃₄ O ₅	12563	8-Isoprostaglandin F2α (8-iso PGF2α)	354.5	C ₂₀ H ₃₄ O ₅	05083
10,11-dihydro-20-dihydroxy-leukotriene B4 (leukotriene B4)	386.48	C ₂₀ H ₃₄ O ₆	12502	20-Hydroxy-prostaglandin F2α (20-hydro PGF2α)	370.5	C ₂₀ H ₃₄ O ₆	04049
Prostaglandin D1 (PGD1)	354.5	C ₂₀ H ₃₄ O ₅	05102	Prostaglandin E1 (PGE1)	354.48	C ₂₀ H ₃₄ O ₅	01442
Prostaglandin D2 (PGD2)	352.4	C ₂₀ H ₃₂ O ₅	01403	8-Isoprostaglandin E1 (8-iso PGE1)	354.5	C ₂₀ H ₃₄ O ₅	04686
Prostaglandin F1α (PGF1α)	356.5	C ₂₀ H ₃₆ O ₅	02685				

Extended Data Fig. 1 | Identification of PGE1 from brain tissue extract. (a) Isolation of endogenous ligand candidates using a combination of boiling, acetone precipitation, and ultrafiltration (3,000 molecular weight cut-off). Fractions were monitored for their Nurr1-enhancing activity using a cell-based luciferase assay system. Nurr1-enhancing activity was unaffected by boiling and acetone precipitation. $n = 3$ independent experiments, Data are presented as mean \pm s.d. (b) Following ultrafiltration, filtrates were fractionated by HPLC column C-18 and each fraction was assayed for Nurr1-activating activities. Fraction 5 contained the most activity and thus was used for the mass spectrometry (MS) analysis. $n = 3$ independent experiments, Data are presented as mean \pm s.d. (c) Candidate compounds that are tested after identification by an ultra-performance liquid chromatography quadrupole time of flight mass spectrometry (UPLC-qTOF-MS/MS).

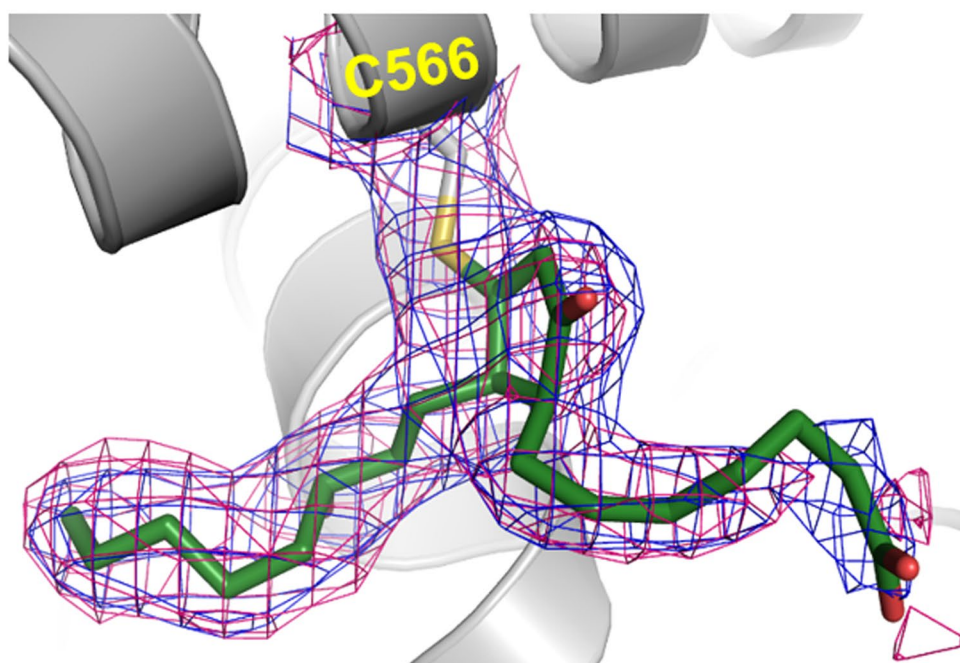
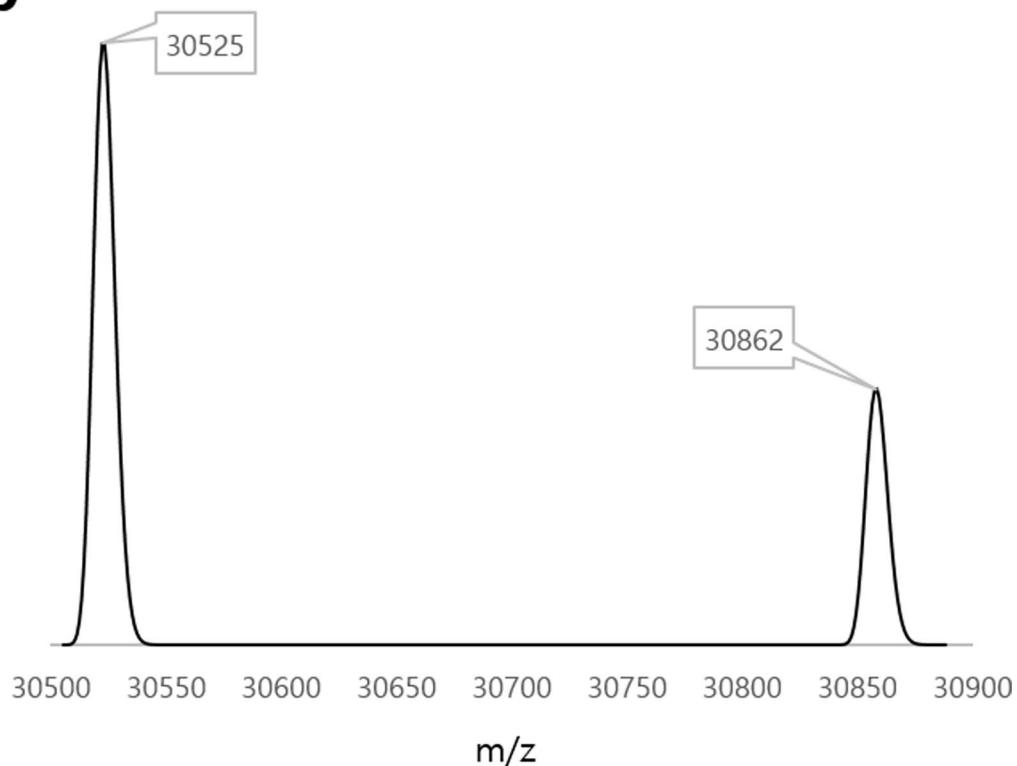


Extended Data Fig. 2 | See next page for caption.

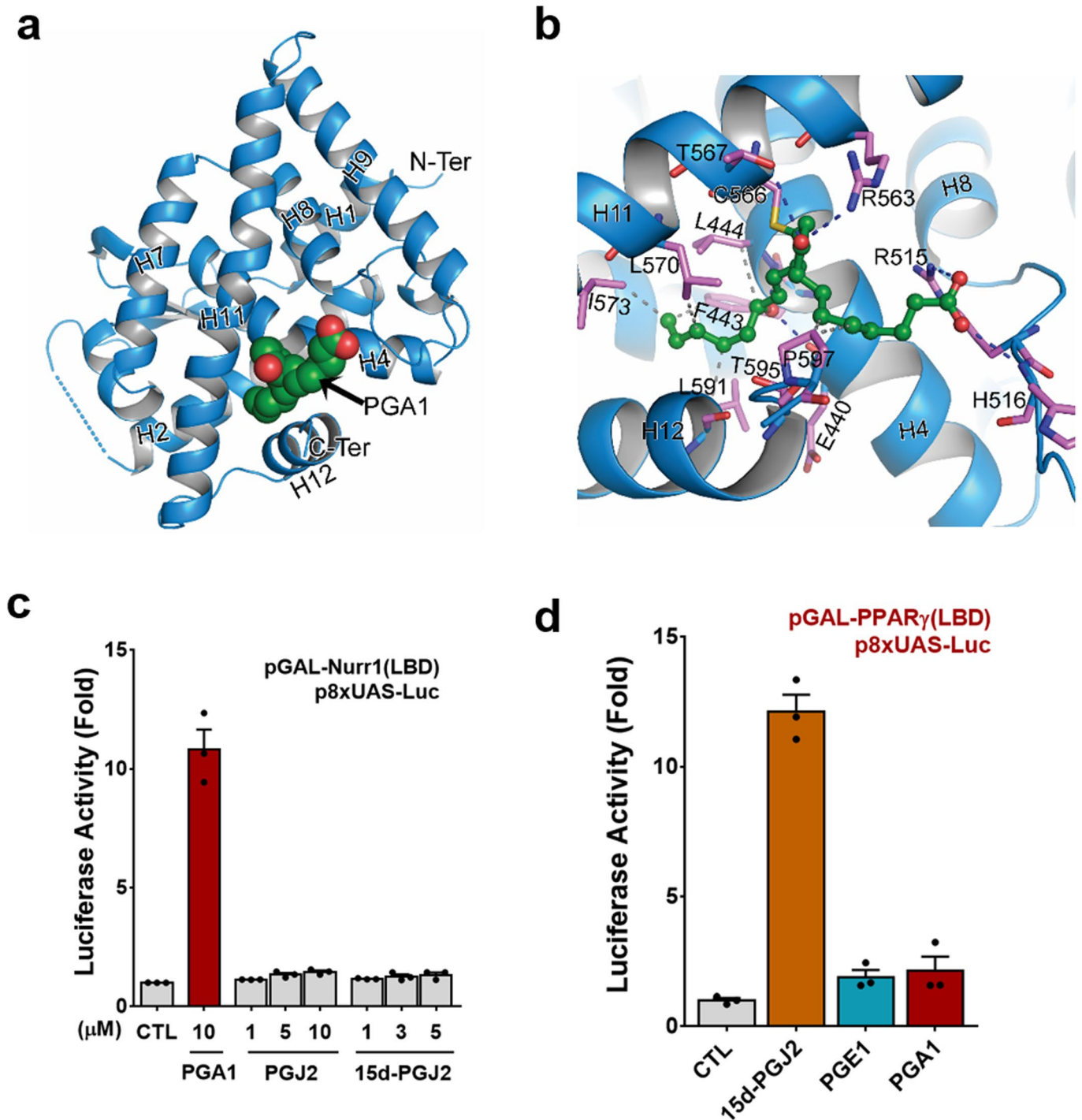
Extended Data Fig. 2 | Direct binding of PGE1 and PGA1 to Nurr1-LBD. (a–f) Molecular interaction of Nurr1-LBD with PGE1 (a and b) and PGA1 (c and d) studied using 2D HSQC NMR titration experiments with uniformly ^{15}N -labeled Nurr1-LBD. (a) Close-up view of a section of the overlay of free Nurr1-LBD (red) and Nurr1-LBD with PGE1 (1:4, green; 1:10, blue), with residues showing chemical shift perturbations (with arrows) or intensity changes (boxed in red) labelled. (b) Selected residues were mapped on the crystal structure of Nurr1-LBD (PDB: 1OVL) in surface representation, with a close-up section (as inset) showing affected helices H4, H11 and H12, with amino acid residues indicated. (c) Close-up view of a section of the overlay of free Nurr1-LBD (red) and Nurr1-LBD with PGA1 (1:5, green; 1:10, blue), with residues showing chemical shift perturbations (with arrows) or intensity changes (boxed in red) labelled. Residues (Leu559, Gln571 and Thr595) showing additional peaks upon PGA1 incubation are marked with asterisks (*). This indicates that the PGE1 (a) and PGA1 (c) interaction with Nurr1-LBD matches the typical two-state binding model ($\text{P} + \text{L} \rightleftharpoons \text{PL}$) and an induced-fit binding model ($\text{P} + \text{L} \rightleftharpoons \text{P}_{\text{open}} \rightarrow \text{P}_{\text{closed}}$), respectively. (d) Mapping of Nurr1-LBD residues perturbed in the presence of PGA1 reveals that both PGE1 (a and b) and PGA1 (c and d) recognize the same binding region on Nurr1-LBD, with maximum perturbation observed in helices H11 and H12. Residues showing chemical shifts and line broadening are coloured in purple while L410 is coloured in red (b and d), as its peak disappeared upon PGA1 binding. (e, f) PGA1 increases the transcriptional activity of Nurr1-based reporter constructs: Nurr1-LBD-dependent (e) and full-length Nurr1-dependent (f) transcriptional activities in SK-N-BE(2)C cells. $n = 3$ independent experiments, Data are presented as mean \pm s.e.m.



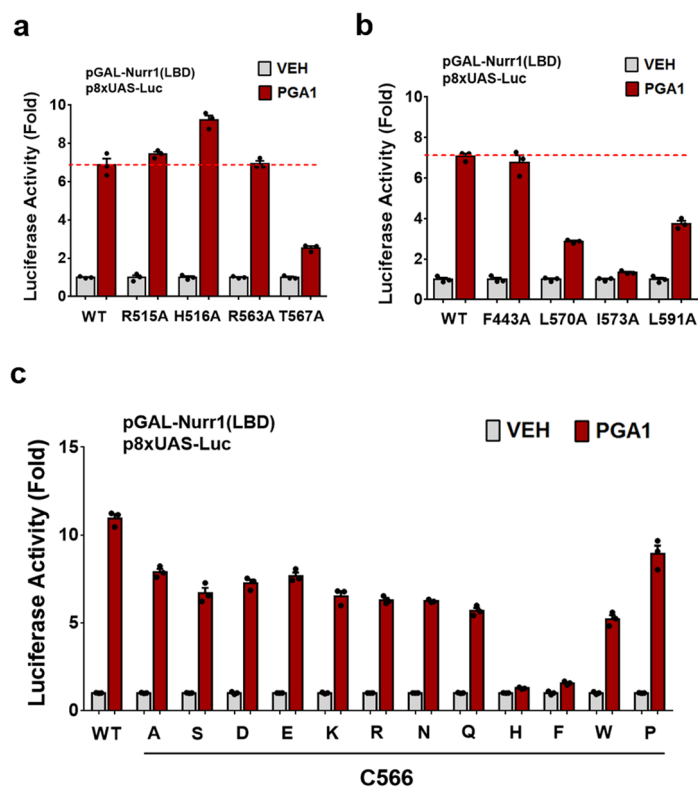
Extended Data Fig. 3 | Chemical shift perturbation plot of Nurr1-LBD upon PGE1 and PGA1 binding. Chemical shift perturbation plot of Nurr1-LBD upon PGE1 (**a**) / PGA1 (**b**) binding (1:10 ratio) and their corresponding peak intensity plots (PGE1 (**c**) / PGA1 (**d**)) revealing residues with perturbed resonances and/or line broadening upon ligand binding. (*) denotes the peak belonging to L410 which disappeared upon PGA1 binding.

a**b**

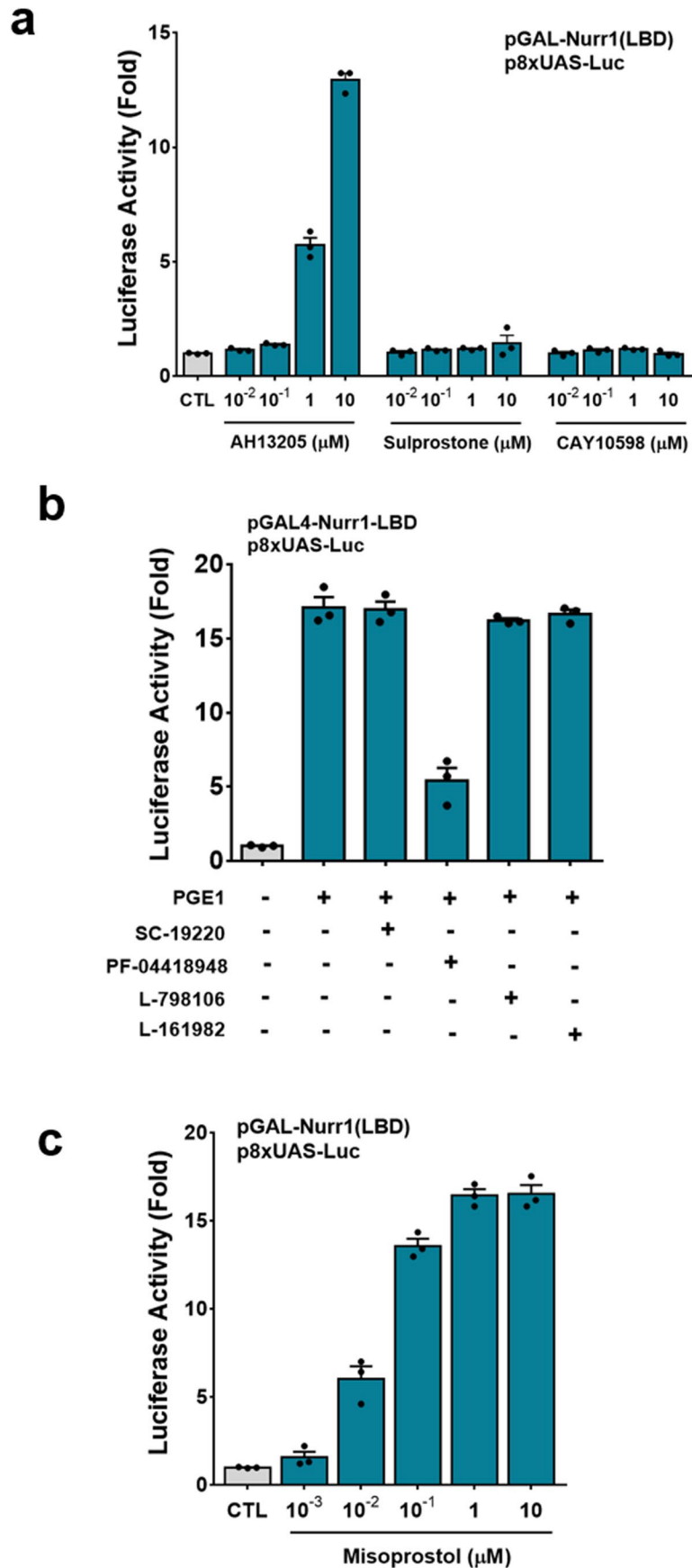
Extended Data Fig. 4 | PGE1 conversion to PGA1 under crystal condition. (a) The overlaid 2Fo-Fc (blue) and composite omit (pink) electron density maps contoured at 1 σ cut-off confirming the conversion of PGE1 to PGA1, evident from the covalent bonding density with Cys566. (b) Mass spectrometry data of PGE1 incubated with Nurr1-LBD under crystallization buffer condition (100 mM MES, pH 5.5 and 200 mM MgCl₂) confirming the conversion of PGE1 to PGA1, as revealed by the covalent complex molecular mass of 30,862 Da (Nurr1-LBD³²⁸⁻⁵⁹⁸ is 30,525 Da and PGA1 is 336.5 Da).



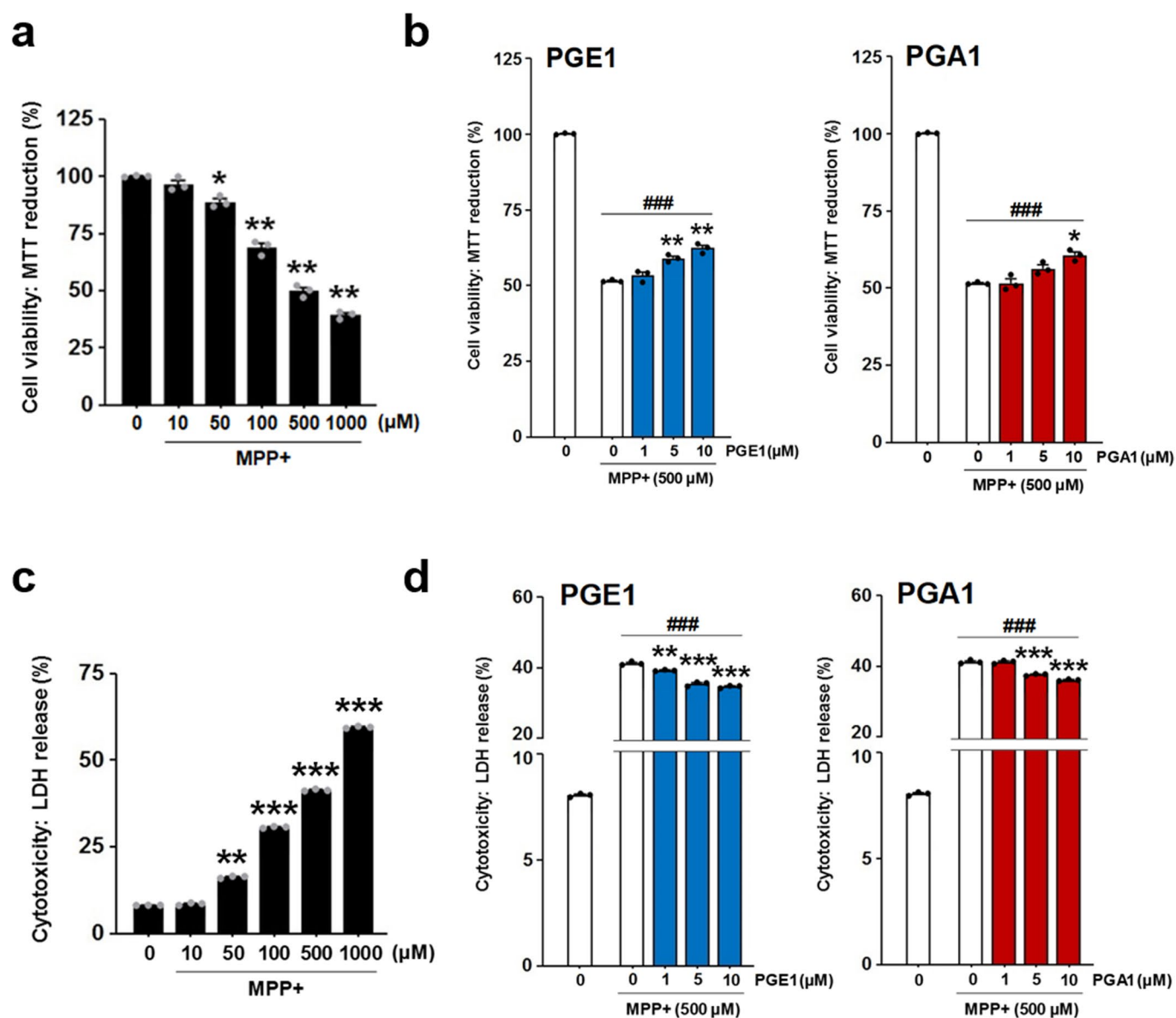
Extended Data Fig. 5 | Crystal structure of PGA1-bound Nurr1-LBD and its molecular and functional analyses. (a) Cartoon representation of Nurr1-LBD (blue) with PGA1 shown in sphere mode. (b) Interactions between PGA1 and Nurr1 residues (labelled) through hydrophobic contacts (grey broken lines) and hydrogen bonds (blue broken lines). Only chain B in the asymmetric unit are shown here, as the electron density for the PGA1 attached to this chain was complete. (c) PGJ2 and 15d-PGJ2 show no effect on the transcriptional activity of Nurr1-LBD. $n=3$ independent experiments, Data are presented as mean \pm s.e.m. (d) 15d-PGJ2 (3 μ M), but not PGE1 (1 μ M) or PGA1 (10 μ M), induces the transcriptional activity of PPAR γ -LBD.



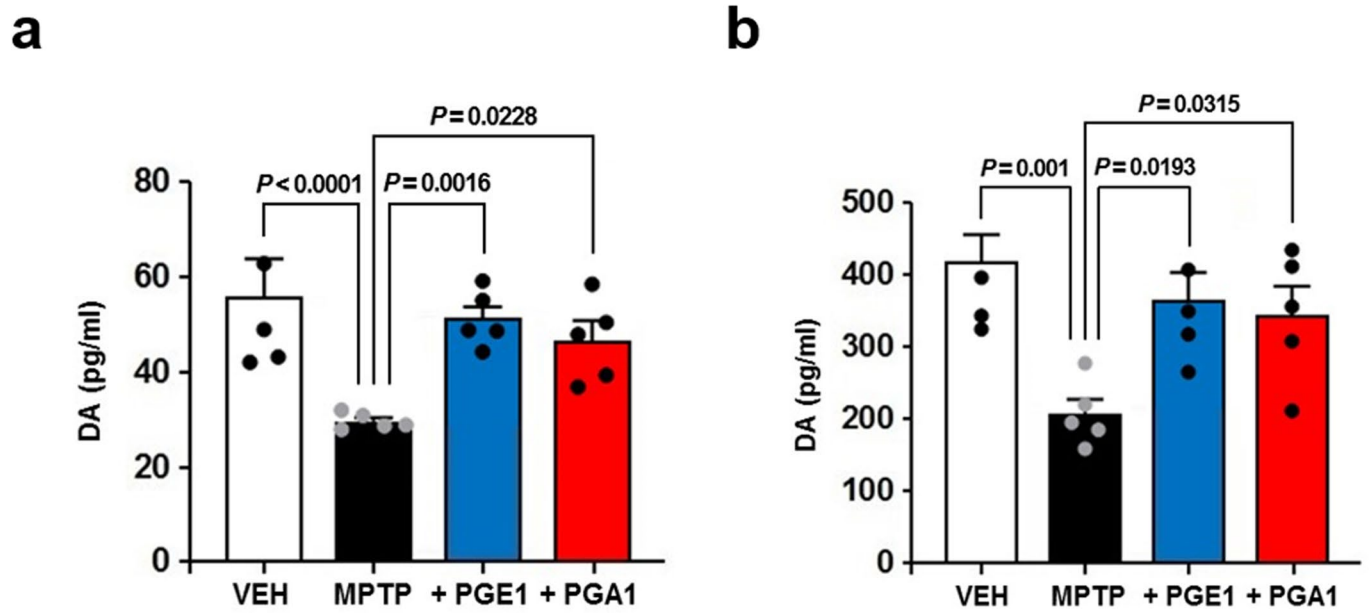
Extended Data Fig. 6 | Effects of mutations at Nurr1 residues interacting with the chain B (Arg515, His516, Arg563, Thr567). (a), with the chain A (Phe443, Leu570, Ile573, Leu591) (b), and effects of mutations at the residue Cys566 (c) on PGA1 (10 μ M)-induced transcriptional activation of Nurr1-LBD in SK-N-BE(2)C cells. $n=3$ independent experiments, Data are presented as mean \pm s.e.m.



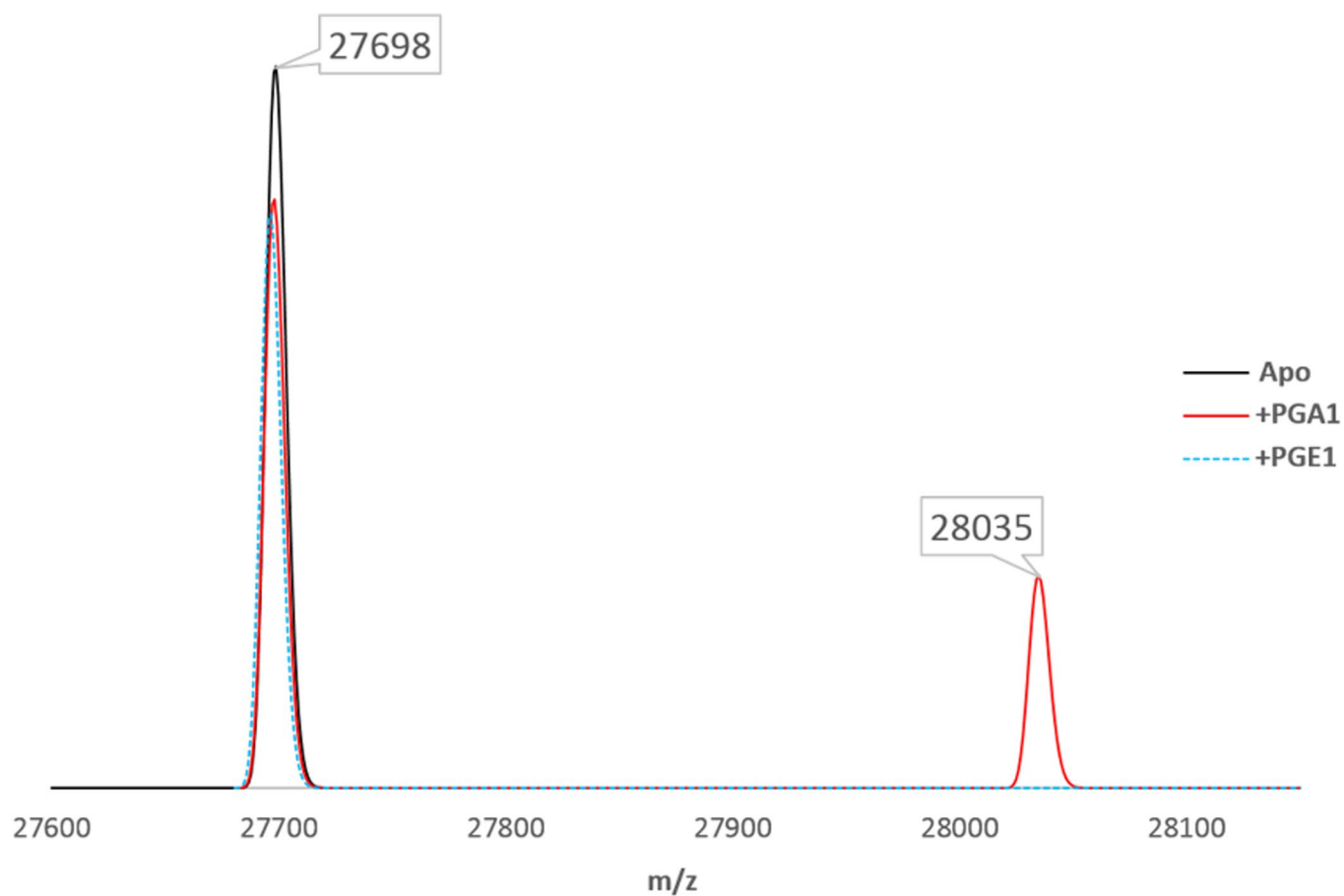
Extended Data Fig. 7 | Effects of EP2 agonists and antagonists on the transcriptional activity of Nurr1-LBD. (a) The EP2 agonist, AH13205 activates Nurr1's transcriptional activity, whereas EP3/EP4 agonists (Sulprostone and CAY10598) do not. (b) EP2 antagonist, PF-04418948 suppresses PGE1-induced transcriptional activation of Nurr1, whereas EP1/EP3/EP4 antagonists (SC-19220, L-798106, and L-161982) do not. (c) The synthetic PGE1 analogue misoprostol, activates Nurr1's transcriptional activity in SK-N-BE(2)C cells. n = 3 independent experiments, Data are presented as mean ± s.e.m.



Extended Data Fig. 8 | Protective effects of PGE1 and PGA1 against MPP⁺ in MN9D cells. (a, b) Determination of protective effects of PGE1 and PGA1 in MN9D cells under MPP⁺-induced oxidative stress measured by MTT reduction. (a) Cells were treated with MPP⁺ (0–1000 μM) for 24 hrs. Cell viabilities assessed by MTT reduction assay show that treatment with 500 μM of MPP⁺ significantly induces 50% of cell death. (b) Pre-treatments with PGE1/PGA1 (24 hrs prior to MPP⁺ treatment) increase cell viability against the MPP⁺ induced oxidative stress in MN9D cells. **P* < 0.05, ***P* < 0.01 compared to 0 μM; ###*P* < 0.001 compared to the absence of MPP⁺, unpaired two-tailed t-test; *n* = 3 independent samples per group. Data are mean ± s.e.m. (c, d) Protective effects of PGE1 and PGA1 measured by LDH release. (c) Cytotoxicity determined by LDH release assay also reveals that treatment with 500 μM of MPP⁺ significantly induces 50% of cell death in MN9D cells. (d) Similar to MTT reduction assay, pre-treatments with PGE1/PGA1 reduce cytotoxicity under the MPP⁺-induced oxidative stress. ***P* < 0.01, ****P* < 0.001 compared to 0 μM; ###*P* < 0.001 compared to the absence of MPP⁺, unpaired two-tailed t-test; *n* = 3 independent samples per group. Data are mean ± s.e.m.



Extended Data Fig. 9 | Effects of PGE1/PGA1 in the MPTP-induced reduction of DA levels. The administration of PGE1/PGA1 significantly restores the MPTP-induced reduction of DA levels in the SN (**a**) and in the striatum (**b**). One-way ANOVA, Tukey's post-hoc test; $n = 5$ per group. Data are mean \pm s.e.m.



Extended Data Fig. 10 | Mass spectrometry data between PGA1 and Nurr1-LBD under NMR condition. Mass spectrometry data confirming the formation of the covalent bond between PGA1 (red line) with Nurr1-LBD³⁵⁶⁻⁵⁹⁸ (28.035 kDa), while PGE1 (blue dotted line) does not form such a covalent attachment under the NMR buffer conditions (20 mM sodium phosphate (pH 7.5) buffer containing 50 mM NaCl, 0.01% NaN₃ in 90% H₂O/10% D₂O). The apo Nurr1-LBD³⁵⁶⁻⁵⁹⁸ (black line) (27.698 kDa) is shown for reference. The molecular weight of PGA1 is 336.5 Da. This also corroborates with the two-state binding and induced-fit model observed from NMR data (Extended Data Fig. 2a, c).

Reporting Summary

Nature Research wishes to improve the reproducibility of the work that we publish. This form provides structure for consistency and transparency in reporting. For further information on Nature Research policies, see [Authors & Referees](#) and the [Editorial Policy Checklist](#).

Statistics

For all statistical analyses, confirm that the following items are present in the figure legend, table legend, main text, or Methods section.

n/a Confirmed

- The exact sample size (n) for each experimental group/condition, given as a discrete number and unit of measurement
- A statement on whether measurements were taken from distinct samples or whether the same sample was measured repeatedly
- The statistical test(s) used AND whether they are one- or two-sided
Only common tests should be described solely by name; describe more complex techniques in the Methods section.
- A description of all covariates tested
- A description of any assumptions or corrections, such as tests of normality and adjustment for multiple comparisons
- A full description of the statistical parameters including central tendency (e.g. means) or other basic estimates (e.g. regression coefficient) AND variation (e.g. standard deviation) or associated estimates of uncertainty (e.g. confidence intervals)
- For null hypothesis testing, the test statistic (e.g. F , t , r) with confidence intervals, effect sizes, degrees of freedom and P value noted
Give P values as exact values whenever suitable.
- For Bayesian analysis, information on the choice of priors and Markov chain Monte Carlo settings
- For hierarchical and complex designs, identification of the appropriate level for tests and full reporting of outcomes
- Estimates of effect sizes (e.g. Cohen's d , Pearson's r), indicating how they were calculated

Our web collection on [statistics for biologists](#) contains articles on many of the points above.

Software and code

Policy information about [availability of computer code](#)

Data collection

The data collection softwares used for the crystal and NMR samples are DA+ and TOPSPIN 2.0, respectively.

Data analysis

For Western blot, image J software (version 1.50b) is used for determining band intensities.
All graphs and data analysis were presented by using GraphPad Prism 8 software.
NMR data analysis was done using NMRFAM-SPARKY 02/12/20, NMRPipe 8.7, and TITan 1.5.
For crystal structure analysis iMOSFLM 7.2.1, SCALA 3.3.22, CCP4 suite 7.0.019, PHENIX 1.8.4, PHASER 2.5.5, REFMAC 5.8.0158, COOT 0.6.2, PyMOL 1.7.2.1, Chimera 1.12 were used.
For mass spectrometry data analysis: Xtract for Qual Browser Thermo Xcalibur 2.2 SP1.48.
Masslynx and Human metabolome database were used for UPLC-qTOF-MS/MS.

For manuscripts utilizing custom algorithms or software that are central to the research but not yet described in published literature, software must be made available to editors/reviewers. We strongly encourage code deposition in a community repository (e.g. GitHub). See the Nature Research [guidelines for submitting code & software](#) for further information.

Data

Policy information about [availability of data](#)

All manuscripts must include a [data availability statement](#). This statement should provide the following information, where applicable:

- Accession codes, unique identifiers, or web links for publicly available datasets
- A list of figures that have associated raw data
- A description of any restrictions on data availability

Coordinates and structure factors have been deposited in the Protein Data Bank under the accession code 5Y41.

Field-specific reporting

Please select the one below that is the best fit for your research. If you are not sure, read the appropriate sections before making your selection.

Life sciences Behavioural & social sciences Ecological, evolutionary & environmental sciences

For a reference copy of the document with all sections, see [nature.com/documents/nr-reporting-summary-flat.pdf](https://www.nature.com/documents/nr-reporting-summary-flat.pdf)

Life sciences study design

All studies must disclose on these points even when the disclosure is negative.

Sample size	Sample sizes were chosen using a target for the power of a statistical test to be applied once the sample is collected.
Data exclusions	No data was excluded from the analyses.
Replication	We tried to replicate at least 3 times for each experiment. All attempts for each experiment were replicated with significant difference in statistical analysis.
Randomization	We randomly allocated all samples and animals without prejudice in this study.
Blinding	For stereotaxic injection and acute MPTP regimen, investigators were not blinded to allocation during experiments and outcome assessment because we initially tested acute MPTP test and compared it with sub-chronic MPTP regimen without blinding. Then, we decided that sub-chronic MPTP is a better model to test neuroprotective effects. Thus, for sub-chronic MPTP regimen, all behavior tests and IHC data acquisition were performed in the assessor and observer blinded fashion.

Reporting for specific materials, systems and methods

We require information from authors about some types of materials, experimental systems and methods used in many studies. Here, indicate whether each material, system or method listed is relevant to your study. If you are not sure if a list item applies to your research, read the appropriate section before selecting a response.

Materials & experimental systems

n/a	Involved in the study
<input type="checkbox"/>	<input checked="" type="checkbox"/> Antibodies
<input type="checkbox"/>	<input checked="" type="checkbox"/> Eukaryotic cell lines
<input checked="" type="checkbox"/>	<input type="checkbox"/> Palaeontology
<input type="checkbox"/>	<input checked="" type="checkbox"/> Animals and other organisms
<input checked="" type="checkbox"/>	<input type="checkbox"/> Human research participants
<input checked="" type="checkbox"/>	<input type="checkbox"/> Clinical data

Methods

n/a	Involved in the study
<input checked="" type="checkbox"/>	<input type="checkbox"/> ChIP-seq
<input checked="" type="checkbox"/>	<input type="checkbox"/> Flow cytometry
<input checked="" type="checkbox"/>	<input type="checkbox"/> MRI-based neuroimaging

Antibodies

Antibodies used	<p>For immunoblot: Mouse Anti-c-myc (Roche Diagnostics GmbH, Cat No. 11667149001, Clone 9E10, Lot No. 28402100, 1:100), Rabbit Anti-Nurr1 (Prepared in our lab, 1:1,000), Rabbit Anti-beta-actin (Abcam, Cat No. ab8227, Lot No. GR3212290-1, 1:5000) were used.</p> <p>For ICC and IHC: Rabbit Anti-Tyrosine Hydroxylase (Millipore, clone LNC1, Cat No MAB318, Lot No 2742733, 1:1000), Goat Anti-Iba-1 (bcam, Cat No. ab5076, Lot No. GR3190885-3, 1:500), and Mouse Anti-NeuN (EMD Millipore, Cat No. MAB377, Clone A60, Lot No. 3075598, 1:500). For secondary, Alexa Fluor 568-conjugated Donkey Anti-Rabbit IgG (Termo Fisher Scientific, Cat No. A10042, Lot No. 1235798, 1:1000), Alexa Fluor 488-conjugated Donkey Anti-Goat IgG (Termo Fisher Scientific, Cat No. A11055, Lot No. 1182671, 1:1000), Alexa Fluor 488-conjugated Donkey Anti-Mouse IgG (Abcam, Cat No. ab150101, GR126425-1, 1:1000), Alexa Fluor 568-conjugated Donkey Anti-Rabbit IgG (Abcam, Cat No. ab175694, GR238033-1, 1:1000), and HRP-Anti-Mouse IgG (Vector Laboratories, Cat No. PI-2000, No X0328, 1:1000) were used.</p>
Validation	<p>Mouse Anti-c-myc antibody was used for immunoblot. Anti-c-myc is a monoclonal antibody to c-myc peptide (clone 9E10). Anti-c-myc recognizes the 9E10 epitope sequence (EQKLISEEDL), derived from the human c-myc protein, notifying its specificity in the manufacture's website. The antibody has been used for publications (Konietzko et al., Neurobiol. Aging 2008; Civiero et al., J Neurochem 2015; Nasim et al., Proc Natl Acad Sci 2010) according to Millipore's website.</p> <p>Rabbit Anti-Nurr1: Antibody was validated in our lab for immunoblot in CHO cells (Leblanc et al., J Vis Exp 2015). It is now commercially available at Sigma-Aldrich (Cat No. ABN1675).</p> <p>Rabbit Anti-Tyrosine Hydroxylase: Supplier validated used for IHC. Antibody has been used for publications (Zhang et al., Nat</p>

Neuroscie 2015; Uemura et al., PLoS GENET 2015; Rompuy et al., Mol Neurodegener 2015 according to Millipore's website.

Goat Anti-Iba-1: Supplier validated used for ICC in the macrophage cell line Mono-Mac 6. Antibody has previously been used for publications (Paiva et al., Glia 2019; Wixey et al., J Neuroinflammation 2019; Hussain et al., Neurobiol Dis 2019) according to Abcam's website.

Mouse Anti-NeuN: Supplier validated use for IHC with mouse brain tissues. Antibody has been used for publications (Moore et al., PLoS Biol 2015; Wu et al., Nat Commun 2015; Wang et al., Mol Neurodegener 2015) according to Millipore's website.

Eukaryotic cell lines

Policy information about [cell lines](#)

Cell line source(s)	Human neuroblastoma SK-N-BE(2)C (Cat. No. CRL-2271) and rat pheochromocytoma PC12 (Cat. No. CRL-7121) cell lines were purchased from ATCC. Murine MN9D cell line was kindly provided by Drs. Michael Zigmund and Julian Jaumotte from the University of Pittsburgh. Rat N27-A cell line was kindly provided by Dr. Curt Freed from the University of Colorado School of Medicine.
Authentication	No authentication procedures for SK-N-BE(2)C, PC12, N27-A, and MN9D cells were used.
Mycoplasma contamination	The cells were tested for mycoplasma contamination every four weeks using Venor™ GeM Mycoplasma Detection Kit (Sigma-Aldrich, Cat No. MP0025). Only mycoplasma-free cells were used for the experiments
Commonly misidentified lines (See ICLAC register)	No commonly misidentified cells were used.

Animals and other organisms

Policy information about [studies involving animals](#); [ARRIVE guidelines](#) recommended for reporting animal research

Laboratory animals	As described in method section, we used male BALB/c mice (8 weeks) for active compound isolation and male C57BL/6 mice (3-month old, 25-30 g) for MPTP-induced animal experiment. Moreover, we also used pregnant C57BL/6 mice for primary dopaminergic neuron culture. All mice were obtained from Jackson Laboratory (Bar Harbor, ME, USA)
Wild animals	No wild animals were used.
Field-collected samples	This study did not use samples collected from the field.
Ethics oversight	Animal care and handling was carried out according to guidelines issued by McLean Hospital's Institutional Animal Care and Use Committee and followed National Institutes of Health guidelines.

Note that full information on the approval of the study protocol must also be provided in the manuscript.